Oligodendrocyte-derived exosomes promote axonal transport and axonal long-term maintenance

Carsten Frühbeis[1$], Wen Ping Kuo-Elsner[1$], Kerstin Barth[1], Leticia Peris[2], Stefan Tenzer[3], Wiebke Möbius[4], Hauke B. Werner[4], Klaus-Armin Nave[4], Dominik Fröhlich[1,5], and Eva-Maria Krämer-Albers*[1]

[1]Institute of Developmental Biology and Neurobiology, Biology of Extracellular Vesicles Group, University of Mainz, 55099 Mainz, Germany

[2]University Grenoble Alpes, Inserm, U1216, Grenoble Institut Neurosciences, 38000 Grenoble, France

[3]Institute of Immunology, University of Mainz, 55131 Mainz, Germany

[4]Max Planck Institute of Experimental Medicine, Göttingen, Germany

[5]present address: Translational Neuroscience Facility and Department of Physiology, School of Medical Sciences, University of New South Wales, Sydney, NSW, Australia.

*corresponding author

[§]equal contribution

Key words: Extracellular vesicles, exosomes, oligodendrocytes, myelin, axon-glia interaction, trophic support, axonal transport, axonal integrity, CNP-null, PLP-null

Short title: Oligodendroglial exosomes facilitate axonal maintenance

Abstract

Neurons extend long axons that require maintenance and are susceptible to degeneration. Long-term integrity of axons depends on intrinsic mechanisms including axonal transport and extrinsic support from adjacent glial cells. The mechanisms of support provided by myelinating oligodendrocytes to underlying axons are only partly understood. Oligodendrocytes release extracellular vesicles (EVs) with properties of exosomes, which upon delivery to neurons improve neuronal viability in vitro. Here, we show that oligodendroglial exosomes support neurons by promoting fast axonal transport, most strikingly under conditions of oxidative stress and nutrient deprivation. Interestingly, oligodendroglial exosome secretion is impaired in two mouse mutants exhibiting secondary axonal degeneration due to oligodendrocyte-specific gene defects. Mutant oligodendrocytes release less exosomes that share a common signature of underrepresented proteins. Notably, mutant exosomes lack the ability to support nutrient deprived neurons and to promote axonal transport. Together, these findings indicate that glia to neuron exosome transfer promotes neuronal long-term maintenance by facilitating axonal transport, providing a novel mechanistic link between myelin diseases and secondary loss of axonal integrity.

Introduction

Extracellular vesicles (EVs) are a heterogeneous group of secreted vesicles that appear to be engaged in a wide range of neural cell communication processes and have been implicated in neural development, maintenance, neurodegeneration and regeneration (1-3). According to their site of biogenesis, EVs can be subclassified as exosomes, which are released from the lumen of secretory multivesicular bodies (MVBs), and microvesicles (MV) being shedded from the plasma membrane (4, 5). By delivering a mixed cargo of biomolecules including nucleic acids to target cells, EVs are able to elicit pleiotropic effects and give rise to plastic modulation of the tissue microenvironment (6). In the central nervous system (CNS), neurons and glial cells release EVs under physiological and pathological conditions. However, the target cell responses and the mode of action of EVs in the CNS are not well understood.

Our previous work demonstrated the transfer of exosomes from myelinating oligodendrocytes to neurons (7, 8). Triggered by neuronal signals, oligodendrocytes release small EVs (sEVs) with features of exosomes derived from MVBs. These MVBs appear prevalent at periaxonal sites in myelinated nerves. Neurons internalize oligodendroglial sEVs by endocytosis (which can occur at somatodendritic and axonal sites) and recover the EV-cargo, thereby importing bioactive molecules. Notably, the metabolic activity of neurons receiving sEVs is increased, in particular under stress conditions (8). In addition, the neuronal firing rate is increased and pro-survival signalling pathways are activated (9). Together, these observations suggest that glia-derived sEVs of exosomal origin mediate neuroprotection and improve neuronal homeostasis.

Neurons exhibit a complex polarized architecture, with axons projecting far away from the neuronal cell body that need to be supplied with energy and newly synthesized molecules. The long-term integrity of myelinated axons depends on oligodendroglial factors, which has been generally described as glial trophic support (10). Mice lacking genes encoding oligodendroglial proteo-lipid protein (PLP) and 2´, 3´-cyclic nucleotide 3´-phosphodiesterase (CNP) develop a secondary progressive axonal degeneration characterized by the formation of axonal swellings (11, 12), which may result from a defect in axonal transport (13). Glial support has been attributed to the supply of axons with energy-rich glycolytic metabolites such as lactate and pyruvate through monocarboxylate transporters MCT1 and MCT2 (14-17). However, the causal relationship between the lack of PLP and CNP, metabolic support, and axonal degeneration is still unknown.

Axonal transport drives cargo along microtubules in both anterograde and retrograde direction and is essential for neuronal homeostasis. It comprises fast axonal transport of vesicular cargo and a slow component for the transport of cytoskeletal components and soluble content (18). Reduced transport rates are an early sign of axonal dysfunction preceding axonal degeneration and are also an early event in human myelin diseases (19-21). As yet, the molecular mechanisms linking glial dysfunction and axonal transport decline are unknown.

Here, we studied the effect of oligodendroglial sEVs on axonal maintenance and examined their impact on fast axonal transport by live-cell imaging of vesicular cargo travelling along axons. We show that adding sEVs to neurons promotes axonal transport most prominently under conditions of cell stress. Intriguingly, we found that the release of sEVs from PLP- and CNP-deficient oligodendrocytes is impaired and that mutant sEVs, which share a common altered proteome signature, are dysfunctional. We conclude that sEVs of exosomal nature delivered from oligodendrocytes to neurons contribute to axonal homeostasis and long-term maintenance by facilitating axonal transport. Secondary axonal degeneration, as observed in PLP- and CNP-deficient mice, is coupled to glial exosome function providing a so far missing link between glial dysfunction, axonal transport and axonal degeneration as seen in various neurological diseases.

Results

Oligodendroglial sEVs promote fast axonal transport

To examine the influence of oligodendroglial exosomes on axonal maintenance, we performed live-imaging of fast axonal transport in cultured hippocampal neurons. We determined the dynamics of vesicles delivering brain-derived neurotrophic factor (BDNF) exemplifying dense core vesicles (22). sEVs were isolated from culture supernatants of primary oligodendrocytes by differential ultracentrifugation. As EV isolation procedures do not selectively purify exosomes, we refer to sEVs when studying these fractions (23), although our previous work indicates that these sEVs largely comprise exosomes derived from MVBs (7, 8, 24). Primary hippocampal neurons expressing BDNF-mCherry were exposed to oligodendrocyte-derived sEVs and recorded by time lapse imaging to determine the effect of sEVs on the movement of BDNF-mCherry-carrying transport vesicles along axons (Figure 1A, B). Quantitative analysis of single vesicle trajectories in kymographs revealed a similar distribution profile of vesicular movement in treatment and sham conditions (Figure 1C). Relative anterograde and retrograde vesicle motion and the percentage of static vesicles was unchanged. Likewise, vesicle velocity was unaffected by sEV-treatment (Figure 1D). In contrast, sEV-treatment significantly decreased the pausing time, which depicts the percentage of pauses exhibited by every single vesicle during its total trajectory (Figure 1E). These data indicate that oligodendroglial sEVs facilitate axonal transport by reducing vesicle pausing time.

We further studied axonal transport under stress conditions by challenging sEV-receiving neurons with oxidative stress, which is commonly associated with neurodegeneration (25). BDNF-mCherry expressing hippocampal neurons were pre-incubated with isolated oligodendroglial sEVs before exposure to oxidative stress for 1 h prior to time-lapse recording (Figure 2A, B). To assess cell-type specific effects, one experimental group of neurons was treated with sEVs derived from HEK293T-cells. Kymograph analysis (Figure 2C-E) revealed a significant increase of anterograde vesicle movement upon treatment with oligodendroglial sEVs compared to control neurons and neurons treated with HEK-sEVs, while retrograde movement was unaffected. Concomitantly, the proportion of static vesicles was decreased in oligodendroglial-sEV treated neurons. Vesicle velocity was not significantly affected, although there was a trend towards lower speed in retrograde direction, which came to statistical significance in neurons treated with HEK-derived sEVs. Notably, the relative pausing time of transport vesicles was considerably reduced in neurons treated with oligodendroglial sEVs. In contrast, HEK-derived sEVs interfered with transport by strongly increasing the vesicle pausing time. Taken together, these results demonstrate that oligodendroglial sEVs promote fast axonal transport by reducing vesicle pauses and enhancing anterograde vesicle movement, most prominently when neurons are subjected to stress. The axonal transport promoting

activity appears specific to oligodendroglial EVs as opposed to EVs of non-oligodendroglial origin.

Oligodendroglial sEVs maintain axonal transport in starving neurons

Next, we studied axonal transport under conditions of nutrient deprivation (by depletion of the media supplement B27) reflecting the withdrawal of neurons from the external supply of growth-promoting factors essential for their maintenance. Primary hippocampal neurons were treated with sEV-conditioned oligodendrocyte supernatant (10K) or sEV-deprived supernatant (100K) as control and subjected to nutrient-deprivation during the last 3 hours of the treatment before time-lapse imaging (Figure 3A). 10K (ND +OL-sEV) and 100K (ND) treatment conditions were identical regarding the presence of oligodendroglial secreted soluble components and only differed in presence or absence of sEVs. Unstressed neurons grown in full culture medium served as reference for optimal conditions. As expected, nutrient deprivation resulted in a significant decline of overall vesicular movement (Figure 3B-E). Intriguingly, axonal transport was almost completely restored in nutrient-deprived neurons in the presence of oligodendroglial sEVs. We observed a significant increase in anterograde as well as retrograde movement and the number of static vesicles was substantially reduced upon sEV-treatment back to the normal unstarved level (Figure 3C). Vesicle velocity is not affected by sEV treatment, though nutrient deprivation per se appeared to increase anterograde vesicle velocity (Figure 3D). Furthermore, the presence of sEVs significantly decreased the pausing periods of vesicles in starving neurons (Figure 3E). Thus, neurons receiving oligodendroglial sEVs are able to maintain axonal transport even under conditions of deprivation from external nutrients.

Exosome secretion is impaired in mice affected by secondary axonal degeneration

We further made use of PLP- and CNP-deficient mice, which are established mouse models of glia-dependent secondary axonal degeneration. It is still unclear how the lack of oligodendroglial PLP and CNP is related to the degeneration of axons. Since PLP and CNP are both sorted into exosomes (7), we investigated exosome release in the null-mice. We first looked in the myelinated tract *in situ* at the appearance of MVBs, resembling the cytoplasmic storage sites of exosomes before their actual release. Oligodendroglial MVBs can be readily detected in ultrathin sections of optic nerve fibres by electron microscopy, although their detection depends on their presence in the plane of the section (Figure 4A). Quantification of MVBs in optic nerve sections revealed a 3.6-fold higher number of oligodendroglial MVBs in PLP-null as compared to wild type mice (Figure 4B), while the number of MVBs was unchanged in CNP-null mice (note that MVBs will be strongly underrepresented in relation to axons in the sections). In wild-type optic nerves, MVBs are prevalent at periaxonal (adaxonal)

sites, which is the site of release for axonal delivery. However, in CNP-null mice MVBs appeared underrepresented in the adaxonal and abaxonal cytoplasmic domain, while they were more frequently detected in cytoplasmic channels within myelin (myelinic channels) and in the cell bodies, suggesting that MVB-trafficking to periaxonal sites is impeded (Figure 4C). On the other hand, MVBs in PLP-null mice were more frequent in myelinic channels, at abaxonal loops, and in cell bodies, indicating an accumulation of MVBs in oligodendrocytes (Figure 4D). These observations demonstrate that oligodendroglial MVBs are mislocalized in myelinated tracts of PLP- as well as CNP-null mice, suggesting a defect in exosome release.

We then examined exosome release in cultured oligodendrocytes derived from PLP- and CNP-null mice. Mutant oligodendrocytes exhibit normal morphological differentiation in culture, express the expected lineage markers, and appeared equally viable, although cell death (as determined by LDH-leakiness into the culture medium) appeared slightly increased in PLP-null oligodendrocytes (Supplementary Figure 1). We isolated sEVs including exosomes from culture supernatants collected from wild-type, PLP-, and CNP-null oligodendrocytes by differential centrifugation and determined the particle number and size by nanoparticle tracking analysis (NTA). The number of released particles was significantly reduced in PLP- and CNP-null oligodendrocytes, while the size distribution was unchanged (Figure 4E). Over 24 hours, wild type, CNP-null, and PLP-null oligodendrocytes secreted 435 [± 26], 262 [± 43], and 214 [± 22] particles in the size-range of 50 to 150 nm per cell, respectively, indicating a ~50 % reduction of sEV release by mutant oligodendrocytes. Western-blot analysis of isolated sEVs normalized to the number of releasing cells revealed that common EV-markers including Alix, Tsg101, Flotillin-1 (Flot1), Hsc/Hsp70, PLP, CNP, and Sirtuin-2 (Sirt2) were decreased in mutant versus wild type sEVs, confirming the decreased release rate (Figure 4F, G). The density of sEVs released by mutant oligodendrocytes appeared normal as demonstrated by density gradient analysis, indicating that the lipid/protein ratio and sEV-subtypes are similar between wild-type and mutant sEVs (Supplementary Figure 2). In summary, these data indicate that PLP- and CNP-null oligodendrocytes secrete considerably lower levels of sEVs/exosomes.

CNP- and PLP-null sEVs share common proteome abnormalities

To investigate potential differences in cargo composition between wild-type and mutant sEVs, we performed a differential proteome analysis of density-gradient purified sEVs by label-free quantitative mass spectrometry (LC-MS). Gradient purified sEVs should be enriched for exosomes and devoid of non-EV components co-sedimenting in 100K pellets. The sEV input into LC-MS was normalized according to the total number of sEV-secreting cells (sEV-pools isolated from 2.3 x 10^8 cells), which originated from independent cell preparations and several mouse brains. Functional annotation to Gene Ontology (GO) parent terms “cellular

components" and "biological processes" assigned the largest fraction of identified proteins to the categories "extracellular exosome" and "transport" (Figure 5A), respectively, indicating that the isolation procedure was efficient.

To reveal alterations in the proteome of sEVs derived from mutant PLP- and CNP-null oligodendrocytes, signal intensities were normalized and expressed in parts per million of total protein (ppm). Differential analysis revealed that a number of proteins were up- or downregulated in mutant versus wild-type sEVs (Figure 5B-D, Supplementary Table 1, Supplementary Figure 3). STRING analysis demonstrates highly interconnected networks among up- or downregulated proteins in CNP- as well as PLP-null sEVs, highlighting the tight relationship between these proteins most likely linked to potentially affected biological pathways (Supplementary Figures 4-7). Interestingly, regulated proteins overlapped to a high degree: 50 out of 80 significantly upregulated proteins and 6 out of 25 downregulated proteins were common between PLP-null and CNP-null sEVs/exosomes (Figure 5C). The downregulated proteins include Annexin A5 (Anxa5), Heat shock-related 70 kD protein 2 (Hsp70-2), Sirtuin-2 (Sirt2), Immunoglobulin superfamily member 8 (Igsf8) and Peptidyl-propyl cis-trans isomerase (FKB1A). Notably, these five candidates belong to the top-ten downregulated proteins in both mutant sEV-types and were downregulated at least 2-5 fold (Figure 5D). Typical sEV markers such as the tetraspanins CD81 and CD63 were detected in similar levels in wild-type and mutant sEVs (Alix and Tsg101 were not identified by LC-MS).

We further focussed on downregulated candidates and attempted to validate the proteins found most prominently reduced in CNP- and PLP-null sEVs by semi-quantitative Western-blotting. sEVs isolated by differential ultracentrifugation were normalized to particle number by NTA before subjecting to Western-blot analysis (Figure 5E). In addition to Hsp70-2, Anxa5, Igsf8, and Sirt2, we examined the sEV markers Flotillin-1 (Flot1), Alix and Tsg101 that were not revealed by LC-MS. Detection levels of PLP were equal between wild-type and CNP-null sEVs and furthermore, levels of CNP were equal between wild-type and PLP-null sEVs, confirming equivalent input of sEV-particles. Flot1, Tsg101, Anxa5 and Sirt2 appeared reduced by trend in PLP-deficient sEVs (Figure 5F). Alix, Hsp70-2, and Igsf8 were reduced in both PLP- and CNP-null sEVs. While these data largely confirm the results obtained by proteomics, it should be noted that the semiquantitative Western blot data exhibit high variance. Together, null-mutant derived sEVs are impaired not only in quantitative but also in qualitative terms. PLP- and CNP-null sEVs exhibit an altered protein composition and furthermore, share a remarkably common signature.

Cargo delivery by PLP- and CNP-null sEVs

We further asked whether mutant-derived sEVs are malfunctioning and fail to deliver signals to neurons. First, we addressed whether PLP- and CNP-null sEVs are able to deliver their

cargo. To this end, we utilized Cre as a reporter of sEV-transfer and cargo retrieval in neurons as established previously (8). Adeno-associated virus (AAV) transduced primary oligodendrocytes expressing Cre-recombinase were co-cultured in Boyden chambers with primary cortical neurons that carry GFP as reporter, which is only expressed after Cre-mediated recombination. Delivery of Cre via oligodendroglial sEVs and recovery in neurons will thus activate the GFP-reporter. Indeed, we observed reporter expression in neurons co-cultured with wild-type as well as PLP- and CNP-null oligodendrocytes, indicating that mutant sEVs were internalized by neurons and released Cre (Figure 6A). However, reporter expression in target neurons was reduced by approximately half upon co-culture with CNP-null oligodendrocytes and PLP-null oligodendrocytes (Figure 6B). Thus, sEVs/exosomes released by PLP- and CNP-deficient oligodendrocytes are competent to deliver cargo to neurons, although the level of transfer is decreased, most likely reflecting the reduced rate of secretion by the mutant donor cells.

PLP- and CNP-null sEVs lack the ability to support nutrient-deprived neurons

Previously, we have shown that oligodendroglial exosomes/sEVs carry neuroprotective activity and mediate stress resistance. Neurons exposed to starvation maintain higher levels of metabolic activity, when treated with sEVs during the nutrient-deprived period (8). To examine if sEV-mediated support of nutrient-deprived neurons is dose-dependent, we performed a dilution-series of sEV-containing (10K) supernatants collected from wild-type oligodendrocytes (Figure 6C). Reduction of sEVs to 60 % of initial particle concentration (100 % = 2.48 x 10^8 +/- 0.12 particles/ml) was sufficient to largely abrogate the sEV-mediated support, comparably to sEV-depleted 100K supernatants. Since sEV-release in CNP- and PLP-null is reduced by roughly half, we hypothesized that the reduced level of sEV transfer from mutant oligodendrocytes would result in loss of support of nutrient-deprived neurons. We treated cortical neurons during starvation with sEV-containing 10K supernatants derived from equal numbers of wild-type, PLP- and CNP-null oligodendrocytes. As described above, the mutant-derived supernatants would contain roughly halved sEV concentration. Analysis of cell viability revealed that wild-type sEV-containing supernatants were able to fully restore the metabolic activity of starving cells, while PLP- and CNP-null sEV-containing supernatants lacked the ability to support nutrient-deprived neurons, as do wild-type derived supernatants that were depleted from sEVs (Figure 6D).

To examine if the observed qualitative differences between wild-type and mutant sEVs could also contribute to the lack of neuronal support, starving cortical neurons were treated with sEV-containing 10K supernatants that were normalized for particle concentration by NTA measurement. Remarkably, particle-normalized PLP- and CNP-null sEVs still lacked the ability of wild-type sEVs to rescue starving neurons (Figure 6E). Taken together, these data

demonstrate that the reduced rate of sEV secretion in null-mutants likely is sufficient to interfere with sEVs providing neuronal support. Moreover, the qualitative defects in sEV composition also lead to functional impairment, showing that PLP- and CNP-null sEVs are lacking key factors essential for neuronal support. Thus, both qualitative and quantitative defects of mutant sEVs contribute to their malfunction and the failure to promote neuronal viability.

PLP- and CNP-null sEVs fail to promote axonal transport

To examine the potency of PLP- and CNP-null sEVs to facilitate axonal transport, we performed live-imaging of BDNF-mcherry carrying vesicles in primary hippocampal neurons subjected to nutrient deprivation as described above (Figure 7A). Neurons were treated with sEV-containing supernatants derived from wild-type, PLP-null, CNP-null oligodendrocytes, and in addition from primary cultured astrocytes. Astrocytes are known to contribute to neuronal functions in manifold ways and hence we included this treatment condition as further control for cell-type specific sEV action. Intriguingly, treatment with sEVs derived from PLP- and CNP-null oligodendrocytes, as well as sEVs derived from astrocytes, did not rescue fast axonal transport in nutrient-deprived neurons (Figure 7B-E). Compared to wild-type sEV-treatment, both anterograde and retrograde movement of transport vesicles was reduced and the pool of static vesicles was increased back to the level of untreated nutrient-deprived neurons (Figure 7C). The vesicle velocity was largely unaffected (Figure 7D, reduction of anterograde vesicle velocity by mutant sEVs should be taken with caution due to high variance of measurements). Furthermore, the pausing-time of moving vesicles was neither reduced by PLP- and CNP-null sEVs nor by astrocyte-derived sEVs (Figure 7E). Thus, the axonal transport promoting activity is specific to sEVs derived from oligodendrocytes as opposed to astrocytes. sEVs derived from PLP- and CNP-deficient oligodendrocytes lack this activity and fail to restore axonal transport during nutrient deprivation.

Discussion

Our study provides new evidence that oligodendrocyte-derived sEVs are critical factors of long-term axonal maintenance. We show that oligodendroglial sEVs promote axonal transport under normal as well as stress conditions, which is essential for the maintenance of axonal integrity. Consistently, CNP- and PLP-deficient mice suffering from secondary axonal degeneration exhibit impaired sEV-release from oligodendrocytes. Mutant-derived sEVs lack the ability to foster the neuronal metabolism and to promote axonal transport. sEV loss of function is accompanied by a common proteomic signature and the reduced abundance of several shared proteins, implicating a set of functionally relevant sEV-cargos. Thus, our study establishes sEV-delivery from oligodendroglia to neurons as a mechanistic route to sustain neuronal integrity and provides a so far missing link between glial dysfunction, axonal transport and axonal degeneration.

Recently, EVs were introduced as signalling entities playing versatile roles in normal brain physiology, during neurodegenerative disease as well as in the context of neuroregeneration (1, 2, 26). EVs are highly heterogeneous regarding their origin and cargo, and once present in the extracellular space, it is almost impossible to technically discriminate between plasma-membrane derived EVs (microvesicles) and endosome-derived EVs (exosomes). A substantial body of evidence based on electron microscopy and biochemical characterization suggests that oligodendroglial sEVs largely reflect exosomes derived from MVBs (7, 8). In situ, these MVBs frequently appear in the inner cytoplasmic loop next to axons, from where they can be released into the periaxonal space and taken up by axons. We thus assume that exosomes reflect the main functional entity in the sEV-isolates carrying axonal transport promoting activity, although we cannot rule out a minor fraction of other sEVs contributing to that effect. Consistently, PLP- and CNP-deficient mice exhibit abnormally distributed MVBs in myelinated nerves, suggesting that indeed a defect in exosome release may underlie the axonal degeneration observed in these mice.

The finding that oligodendroglial sEVs influence axonal transport provides mechanistic insight of how sEVs, or exosomes, can affect subcellular processes and contribute to overall neural homeostasis. How EVs transmit biological information and execute their functions in target cells is largely unknown (27). Likewise, we can only speculate about the mode of action by which oligodendroglial sEVs promote axonal transport. According to previous work, neurons endocytose oligodendroglial sEVs even at axonal sites and the cargo is bioactive upon internalization (8), suggesting that delivered biomolecules may be involved. Moreover, sEVs appear to modulate neuronal signalling pathways by stimulating phosphorylation of Akt, JNK, and GSK-β (9). Intriguingly, these kinases are known to regulate axonal transport largely by controlling vesicle-associated motor proteins or their adaptors (18, 28). It therefore seems likely that oligodendroglial sEVs directly act on axonal transport via kinase-mediated motor-

protein control. Under optimal growth conditions and full energy supplies, we observed shorter transport vesicle pauses shortly after sEV application (30 min) independent of vesicle directionality or velocity, indeed suggesting a kinase-mediated effect on motor activity. In stress experiments, neurons were pre-treated with sEVs for several hours before the challenge to mimic persisting sEV availability, as presumed to occur *in vivo*, where neurons are thought to continuously receive exosomes from neighbouring myelinating oligodendrocytes in activity-dependent fashion. Though the sEV-cargo (small molecules, metabolites or proteins) may well affect axonal transport directly, it is also possible that sEVs exhibit a preconditioning activity (by activation of signalling pathways or by providing protective molecules) allowing the neurons to maintain a homeostatic state even under demanding conditions. However, whether sEVs promote axonal transport via kinase regulation or the delivery of specific cargoes (or a combination of both) remains to be established in the future.

Intriguingly, sEV-release by oligodendrocytes is impaired in PLP- and CNP-deficient mice, which undergo secondary axonal degeneration, and mutant-derived sEVs lack functional activity. These findings provide compelling genetic evidence that glia to neuron exosome transfer is a mode of glial support required for long-term axonal integrity. Glial support is related to the supply of neurons with energy-rich metabolites important to satisfy the enormous energy demands associated with neural activity (29, 30). Mature myelinating oligodendrocytes can exist as purely glycolytic cells and deletion of oligodendroglial monocarboxylate transporter MCT1, delivering lactate and pyruvate, causes axonal damage (14, 15). However, how PLP- and CNP-deficiency does interfere with the delivery of energy substrates remained less clear so far. Axonal pathology in these mice is characterized by the development of axonal swellings filled with organelles indicating a defect in axonal transport (11, 12). In fact, axonal transport has been shown to be affected in PLP-null mice, while the underlying mechanism remained in the dark (13). Essentially, impaired exosome release in PLP- and CNP-null oligodendrocytes and the failure of mutant-derived sEVs to promote axonal transport provides a mechanistic link between glial dysfunction and axonal degeneration. The delivery of oligodendroglial exosomes to axons, likely concomitant to a supply with energy substrates, appears to be required to sustain axonal health in long-term.

How does PLP- and CNP-deficiency affect exosome release and function? Based on our observation that MVB number and localization is affected, we assume that the malfunction originates on the glial side resulting in defective exosome biogenesis and MVB transport. It has been shown that in absence of CNP the cytoplasmic (myelinic) channels through the myelin sheath are broken down, interfering with cargo transport from the oligodendrocyte cell body to the cytoplasmic loop adjacent to the axon (31). Consistently, MVBs in CNP-null mice are redistributed to the cell body and less frequently placed at their release site in the periaxonal cytoplasmic loop. Accumulation of MVBs in PLP-null mice may hint to a defect in

MVB maturation, which could be related to the tetraspan properties of PLP and its ability to bind and recruit cholesterol (32). In both mutant lines, we observed a decrease in exosome release by roughly 50 % as well as qualitative abnormalities, which each by itself appear sufficient to account for the loss of the neuronal support function and hence augment each other. Remarkably, five among the most strongly down-regulated exosomal proteins identified by proteomics were identical between PLP and CNP mutant exosomes, thus representing exciting candidates of potential functional relevance. Of note, the chaperone Hsp70-2 and the co-chaperone FKBP1 assist protein folding and thus may be important for axonal proteostasis and neuroprotection (33, 34). This would be consistent with the idea that exosomes deliver macromolecules including heat shock proteins conferring stress resistance to axons, which intrinsically lack the ability to modulate the stress response (35). Igsf8 interacts with CD81 and CD9 in tetraspanin-enriched microdomains and recently was implicated in targeting of perivascular EVs to osteoprogenitor cells, although in this instance Igsf8 was located on the recipient cells (36). It is well possible that Igsf8 may play a role in targeting oligodendroglial exosomes to neurons. However, the individual functional contribution of these candidate proteins to the support of axonal transport and axonal maintenance needs to be addressed in more detail in future studies.

In conclusion, our study establishes oligodendrocyte-neuron exosome transfer as a mechanism of glial support required for long-term axonal maintenance by facilitating axonal transport. By this means, metabolic support provided by the supply of energy substrates is complemented by molecular support through the delivery of larger biomolecules via exosomes, maintaining neuronal homeostasis and sustaining axonal projections. Declining axonal transport precedes axonal degeneration observed in demyelinating diseases and is also a common hallmark of neurodegeneration (20, 37). Thus, our study provides a previously unrecognized mechanistic link between glial dysfunction and impairment of axonal transport as an initial trigger of axonal damage and may open new avenues to therapeutically interfere with axon degeneration observed in a broad range of neurodegenerative diseases.

Material and Methods

Antibodies and reagents

Antibodies used were as follows: mouse anti-O4 and mouse anti-O1 (38), rat anti-PLP (clone aa3), mouse anti-CNPase (11-5B, Sigma), mouse anti-GFAP (1B4; BD), rabbit anti-Iba1 (Wako), rabbit anti-Flot1 (Sigma), mouse anti-AIP1/Alix (49; BD), mouse anti-Tsg101 (4A10; GeneTex), mouse anti HSP70 (clone 7, BD), rabbit anti-Igsf8 (Abcam), rabbit anti-Anxa5 (Abcam), rabbit anti-SIRT2, (Abcam), rabbit anti-hrGFP (Stratagene), Carbocyanin and HRP secondary antibodies (Dianova), Alexa secondary antibodies (Invitrogen).

Animals and cell culture

Experiments were in compliance with the animal policies of the University of Mainz, approved by the German Federal State of Rheinland Pfalz, in accordance with the European Community Council Directive of November 24, 1986 (86_609_EEC).

Mouse strains used were: 1) wild type C57Bl/6-N, 2) $CNP^{Cre/Cre}$ (CNCE) (12) and 3) $PLP^{-/-}$ (KPLP) (11, 39).

Primary oligodendrocytes (pOL) were prepared from embryonic day E14.5 mice as described before (40) or from postnatal day 7-8 mouse brains using the MACS cell separation technology using the Neural Tissue Dissociation Kit and anti-O4 MicroBeads (Miltenyi Biotec) according to the manufacturer's protocol. Briefly, primary oligodendrocytes were isolated from whole brain suspension by magnetic-activated cell sorting via anti-O4 antibodies coupled to magnetic beads and plated at a density of 3 x 10^6 cells/6 cm culture dish. Cells were cultured up to 5 days in vitro (DIV) in oligodendrocyte culture medium: NeuroMACS, 20 ml/l NeuroBrew-21 (Miltenyi Biotec), 2 mM L-glutamine, 10 ml/l 100x Pen-Strep (63.2 µg/ml Penicillin G K-salt; 135 µg/ml Streptomycin sulphate, Gibco). While the MACs cell separation protocol provides cells more rapidly within a few days, both methods result in oligodendrocytes with identical characteristics. To generate oligodendrocyte-conditioned supernatants for application in axonal transport or cell viability assays, O4-sorted oligodendrocytes were kept for 48 h in Neurobasal feeding medium before harvesting and further processing to obtain sEV-containing or sEV-depleted supernatants (see below).

Primary cortical neurons were prepared from E14.5 brain hemispheres as described before (41). For primary hippocampal cultures, hippocampi were dissected from brain hemispheres of E18 embryos, treated with 1 % trypsin for 4 min at 37 °C, washed in Hank's balanced salt solution containing $MgSO_4$ (HBSS+), and dissociated in pre-warmed DNase by repeated passage through a constricted Pasteur pipette until homogenous. Cell suspension was washed twice by the addition of HBSS+ and subsequent centrifugation at 130 x g, 4 °C for 10 min.

Cortical and hippocampal neurons were cultured in Neurobasal feeding medium: Neurobasal (Gibco), 20ml/l B27 (Invitrogen), 0.5 mM L-glutamine, 10 ml/l 100x Pen-Strep (63.2 µg/ml Penicillin G K-salt; 135 µg/ml Streptomycin sulphate, Gibco). During the first 24 h of culture 12.5 µM glutamate (Sigma) was added to the medium.

Primary astrocytes were derived from E14.5 glial cultures as a byproduct of the primary oligodendrocyte preparation. After shaking off oligodendrocytes from astrocyte monolayers, astrocytes were detached by trypsination (0.01 % trypsin, 0.02 % EDTA), plated in 6 cm dishes coated with Poly-L-Lysine (Sigma) and grown to confluency.

HEK293T cells were cultured in DMEM + 10 % FCS and 1 mM sodium pyruvate.

Transfection

Hippocampal neurons were transfected with a plasmid encoding BDNF-mCherry (kindly provided by F. Saudou, Institute des Neurosciences, Grenoble, France) by nucleofection using the AMAXA Mouse Neuron Nucleofector Kit (Lonza). Each transfection was performed with 1.5 x 10^6 hippocampal neurons and plated on three video microscopy dishes (ibidi).

AAV generation, cell infection, and Boyden chamber co-culture

Recombinant AAVs bearing the Cre-recombinase or the hrGFP reporter gene were generated as described previously (8, 42). Primary oligodendrocytes (prepared from E14.5 mice) and cortical neurons were infected by adding 1 µl (5x$10^{7–8}$ vg) to the cell culture medium 6 days before the co-culture experiment. Media was exchanged 24 h after the transduction to remove excess virus particles. Then, oligodendrocytes (DIV 7, 1.8 x 10^6 cells per inset) were co-cultured with cortical neurons (0.7 x 10^6 per well) in Boyden chambers (Six-well companion plates (1 µm pores) and six-well cell culture inserts, BD Falcon). After 24 hours, lysates were prepared from the cortical neurons growing in the bottom well.

sEV isolation and collection of sEV-conditioned supernatants

Culture supernatants were collected over a period of 48 h under serum-free conditions and sEVs were isolated by differential centrifugation as described before (8). Briefly, culture supernatant was cleared from dead cells and debris by successive centrifugation for 10 min at 130 x g and 30 min at 10.000 x g and 4°C in a fixed angle rotor (220.78, Hermle). sEVs remaining in the supernatant were pelleted by ultracentrifugation in polyallomer tubes (Beckman Coulter) for 2 h at 100.000 x g and 4°C (SW40 rotor, 27.000 rpm, RCF (max) 130.000, k-factor 301.4, Beckman Coulter). sEV pellets were resuspended in PBS for nanoparticle tracking analysis (NTA) or SDS-PAGE sample buffer for Western blot analysis. Extensive characterization of oligodendroglial sEVs has been performed previously (7-9) and

the quality of isolated sEVs was regularly checked by NTA and Western blotting. For axonal transport experiments under normal or oxidative stress conditions (see below), sEVs comprising exosomes were resuspended in PBS before being applied to neurons. In nutrient-deprivation experiments, sEV-containing 10.000 x g supernatants (10K) or sEV-depleted 100.000 x g supernatants (100K) lacking the B27 supplement were applied to neurons. sEV normalization was performed according to the number of sEV-producing cells or the number of particles determined by NTA. In case of control sEVs derived from HEK293T cells or primary astrocytes (which are much larger cells compared to oligodendrocytes), sEV-input was according to the same the volume of supernatant harvested from confluent cells covering the same area.

For LC-MS analysis, sEVs were subjected to sucrose density gradient centrifugation to further purify exosomes. Briefly, culture supernatants (serum-free) were collected from a total of approximately 2.3 x 10^8 cells over three subsequent periods of 24 h and subjected to differential centrifugation as described above. In the 100,000 g run, sEVs were centrifuged onto a 200 µl sucrose cushion (1.8 M in TBS) for 2 h at 27,000 rpm and 4 °C in the SW40 rotor. Subsequently, the cushion was diluted and loaded on top of a continuous gradient (0.3-1.8 M sucrose in TBS) followed by centrifugation for 16 h at 27,000 rpm and 4 °C in the SW40 rotor. Density of the fractions was determined using a refractometer (Atago Master-T/2T). Exosome-enriched fractions 5-8 were collected (Supplementary Figure 2) and diluted in TBS and centrifuged at 47,000 rpm in a TLA55 rotor (RCF (max) 130.000, k-factor 90.4, Beckman Coulter) for 1 h. Final exosome pellets were resuspended and directly subjected to trypsin digestion and LC-MS.

Nanoparticle tracking (NTA)

sEVs (100,000 x g pellets) derived from 1.2 x 10^7 oligodendrocytes were resuspended in PBS and analyzed using the Nanosight LM10 system equipped with the green laser (532 nm) and the syringe pump and Nanosight 2.3 software (Malvern) at 23 °C (temperature control). Following settings were used: Camera control in standard mode (camera level 16), particle detection in standard mode (screen gain 16, detection threshold 6, and minimum expected particle size auto). Script control was used (Repeatstart, Syringeload 500, Delay 5, Syringestop, Delay 15, Capture 30, Repeat 4). Five 30 s videos were recorded, particles were tracked (batch process), and average values were formed. Particle concentration was related to the volume of culture supernatant (particles/ml) or the number of secreting cells (particles/cell).

sEV treatment and stress conditions for axonal transport assays

Imaging of axonal transport was performed on BDNF-m-cherry transfected primary hippocampal neurons. sEV treatment, oxidative stress and nutrient deprivation conditions were performed according to (8). sEV input was normalized according to the numbers of secreting cells: sEVs derived from 3 x 10^6 sEV-secreting oligodendrocytes were added to 0.5 x 10^6 neurons. Unstressed hippocampal neurons were treated with 100K pelleted sEVs 30 min before live cell imaging. For imaging axonal transport under oxidative stress conditions, neurons were treated with 100K pelleted sEVs for 12 h followed by addition of 15 µM H_2O_2 (Roth) for 1 h and live cell imaging. Control cells received an equal volume of PBS before stress exposure. Nutrient deprivation of neurons was performed by depletion of B27-supplement from the culture medium. Before nutrient-deprivation, neurons were pre-incubated with oligodendrocyte-conditioned culture supernatant containing sEVs and B27 supplement (10K supernatant) for 12 h, followed by a medium exchange to B27-depleted, sEV-containing 10K supernatant for 3 h. Control cells were treated accordingly with oligodendrocyte-conditioned 100K supernatant depleted from sEVs.

Video microscopy

Hippocampal neurons were imaged at DIV 2 or DIV 3 after isolation and transfection using the Zeiss Axiovert 200M microscope equipped with a 63x oil-immersion lens or the Leica TCS SP5 microscope equipped with a 100x oil-immersion lens. During imaging, cells were kept at 37°C and 5 % CO_2. Time-lapse recordings were acquired by scanning single plane images every 0.5 - 3 seconds with a total of 200 frames. Data were quantified using the *ImageJ* software with the *Multi Kymograph* plugin.

Cell viability/metabolic activity assay

Cortical neurons seeded at a density of 7.4 x 10^4/cm^2 were treated in absence of B27-supplement for 15-17 h with oligodendrocyte-conditioned 10K or 100 K supernatants, which contain sEVs or are depleted from sEVs, respectively. Despite the presence or absence of sEVs, these supernatants are identical regarding other secreted oligodendroglial factors that potentially could influence neurons. For normalization, sEVs derived from an equal number of producing cells (3x10^6 cells per treatment condition) or an equal number of particles as determined by NTA were applied to neurons. For dose-response analysis, 10 K supernatants (2.48 x 10^8 +/-0.12 particles/ml = 100 %) were diluted in medium to a relative concentration of 80, 60, 40, and 20 % or depleted from sEVs (100K = 0 %). To normalize particle concentration between wild-type, CNP-null, and PLP-null sEVs, 10K supernatants were concentrated by ultrafiltration (Amicon, 100 kD filter) and particle concentration was adjusted according to NTA

measurement to 2.6 x 10^8 particles/ml for treatment of nutrient-deprived neurons (743 particles/neuron). Metabolic activity of neurons was determined by the MTT assay. Briefly, 0.75 mg/ml 3-(4,5-dimethylthiazol-2-yl)-2,5-diphenyltetrazolium bromide (MTT, Sigma) was added to culture medium for 2 h. Formazan crystals formed were solubilized in a buffer containing 40 % (v/v) dimethyl-formamide (Sigma), 10 % (w/v) SDS, and 2 % (v/v) acetic acid overnight. The absorbance was measured at 562 nm using a plate reader (Tecan Infinite M200 pro).

Cell lysates, Western blotting, and Immunocytochemistry

Cells were scraped in 10 mM Tris pH 7.4, 150 mM NaCl, 1 mM EDTA, 1 % Triton X-100 and protease inhibitor cocktail (Roche complete) on ice. Nuclei were pelleted by centrifugation for 10 min at 300 x g. Cell lysates and sEV/exosome samples (derived from 1.6x10^7 cells) were subjected to 12 % SDS-PAGE and Western blotting (Biorad) or to 4-12 % (Bis-Tris gel) and Western blotting (NuPAGE, Life Technologies). Proteins were blotted onto a PVDF membrane, which was subsequently blocked with 4 % milk powder and 0.1 % Tween in PBS. Membranes were sequentially incubated with primary and HRP-coupled secondary antibodies and proteins were detected using chemiluminescence reagents (Luminata Crescendo, Millipore) and X-ray films. Films were scanned and analysed using ImageJ software (National Institutes of Health). Immunocytochemical staining of cells was performed as described (41). Fluorescence images were acquired using a fluorescence microscope (DM6000m, Leica) and processed with Image J.

Electron microscopy

Adult mice (age 10 weeks) were fixed by perfusion with 4 % formaldehyde (Serva) and 0.2 % glutaraldehyde (Science Services) in 0.1 M phosphate buffer containing 0.5 % NaCl. Gelatin-embedded pieces of optic nerves were infiltrated in 2.3 M sucrose in 0.1 M phosphate buffer over night. Pieces of optic nerve samples were mounted onto aluminum pins for ultramicrotomy and frozen in liquid nitrogen. Ultrathin cryosections were prepared using a cryo-ultramicrotome (UC6 equipped with a FC6 cryobox, Leica). Sections were analyzed with a LEO EM912 Omega (Zeiss). Digital micrographs were recorded with an on-axis 2048x2048-CCD camera (TRS). To quantitate MVBs, cryosections of optic nerves from three different animals per genotype were analyzed. Ten images were taken from every sample at 8000x magnification each covering an area of 11.5 µm x 11.5 µm, summing up to a total area of 1322,5 μm^2 per sample. On every image the number and localization of MVBs were evaluated and the total number of myelinated axons was counted. The number of MVBs is calculated relative to the number of axons in the imaged field.

LC-MS

For mass spectrometry analysis, sEVs were collected from a total of 2.3 x 10^8 primary oligodendrocytes (>3 independent cell preparations, each derived from a pool of >10 individual embryonic mouse brains) and enriched for exosomes by successive differential centrifugation and sucrose density gradient centrifugation as described above. Density-gradient purified exosomes were pelleted in 1.5 ml LoBind Eppendorf tubes and solubilized in 50 mM ammonium bicarbonate, 0.2 % RapiGest (Waters, Eschborn, Germany). Proteins were reduced by adding 5 mM DTT (45 min, 56 °C) and free cysteines alkylated with iodoacetamide (Sigma, Taufkirchen, Germany; 15 mM, 25 °C, 1 h in dark). Sequencing grade trypsin (Promega, Mannheim, Germany) was added and the samples were incubated overnight at 37 °C. After digestion, RapiGest was hydrolyzed by adding 10 mM HCl (37 °C, 10 min) and the resulting precipitate was removed by centrifugation (13 000 x g, 15 min, 4 °C). The supernatant was transferred into an autosampler vial for peptide analysis by LC-MS.

Nanoscale LC separation of tryptic peptides was performed with a nanoAcquity system (Waters Corporation) equipped with an ethylene bridged hybrid (BEH) C18 analytical reversed-phase column (1.7 µm; 75 µm by 150 mm) (Waters Corporation) in direct injection mode. 2 µl of tryptic digest was injected per technical replicate. Mobile phase A was water containing 0.1% (vol/vol) formic acid, while mobile phase B was acetonitrile (ACN) containing 0.1% (vol/vol) formic acid. The peptides were separated with a gradient of 3 to 40% mobile phase B over 60 min at a flow rate of 300 nl/min, followed by a 10-min column rinse with 90% of mobile phase B. The columns were reequilibrated under the initial conditions for 15 min. The analytical column temperature was maintained at 55°C. The lock mass compound, [Glu1]-Fibrinopeptide B (500 fmol/µl), was delivered by the auxiliary pump of the LC system at 300 nl/min to the reference sprayer of the NanoLockSpray source of the mass spectrometer.

Mass spectrometric analysis of tryptic peptides was performed using a Q-TOF Premier mass spectrometer (Waters Corporation, Manchester, United Kingdom). For all measurements, the mass spectrometer was operated in V-mode with a typical resolution of at least 10,000 FWHM (full width half maximum). All analyses were performed in positive-mode electrospray ionization (ESI). The time of flight analyzer of the mass spectrometer was externally calibrated with a NaI mixture from m/z 50 to 1,990. The data were acquisition lock mass corrected using the doubly charged monoisotopic ion of [Glu1]-Fibrinopeptide B. The reference sprayer was sampled with a frequency of 30 s. Accurate mass LC-MS data were collected in data-independent modes of analysis. The spectral acquisition time in each mode was 0.7 s with a 0.05-s interscan delay. In low-energy MS mode, data were collected at a constant collision energy of 4 eV. In elevated-energy MS mode, the collision energy was ramped from 25 to 55 eV during each 0.6-s integration. One cycle of low- and elevated-energy data was acquired every 1.5 s. The radio frequency amplitude applied to the quadrupole mass analyzer was

adjusted so that ions from m/z 350 to 2,000 were efficiently transmitted, ensuring that any ions observed in the LC-MS data less than m/z 350 were known to arise from dissociations in the collision cell. All samples were analyzed in quintuplicate.

Data processing

Continuum LC-MS data were processed and searched using ProteinLynx GlobalSERVER version 3.0.2 (Waters Corporation). Protein identifications were obtained by searching a custom compiled database containing sequences of Uniprot Swissprot Mouse Reference Proteome database (17.005 entries). Sequence information of enolase 1 (S. cerevisiae) and bovine trypsin were added to the databases to normalize the data sets or to conduct absolute quantification as described previously (43). Guideline identification criteria were applied for all searches. The LC-MS data were searched with a 10-ppm precursor and 20-ppm product ion tolerance, respectively, with one missed cleavage allowed and fixed carbamidomethylcysteine and variable methionine oxidation set as the modifications.

Statistical analysis

Quantitative data are means ±SEM of at least three independent experiments. Statistical analysis was performed when n>4 using Graph Pad Prism Software X8. Data were subjected to normality tests Anderson-Darling, D'Agostino-Pearson, Shapiro-Wilk, and Kolmogorov-Smirnov and considered normally distributed if passing all four tests. For axonal transport assays data groups of individual recorded cells collected from at least three independent experiments were compared using two-tailed, unpaired Student's t-test followed by Holm-Sidak correction for multiple comparisons. MTT assay for dose response analysis was tested by oneway ANOVA followed by Dunn's multiple comparison test. Data derived from MTT-assays comparing neuronal metabolic activity in response to wild-type and mutant sEVs were analysed by two-tailed, unpaired Student's t-test.

Data Availability

The data that support the findings of this study that are not included within the paper and its supplementary information files are available from the corresponding author upon reasonable request.

References

1. Budnik V, Ruiz-Canada C, Wendler F. Extracellular vesicles round off communication in the nervous system. Nat Rev Neurosci. 2016;17(3):160-72.
2. Krämer-Albers EM, Hill AF. Extracellular vesicles: interneural shuttles of complex messages. Curr Opin Neurobiol. 2016;39:101-7.
3. Krämer-Albers EM, Ping Kuo-Elsner W. Extracellular Vesicles: Goodies for the Brain? Neuropsychopharmacology. 2016;41(1):371-2.
4. Raposo G, Stoorvogel W. Extracellular vesicles: exosomes, microvesicles, and friends. The Journal of cell biology. 2013;200(4):373-83.
5. van Niel G, D'Angelo G, Raposo G. Shedding light on the cell biology of extracellular vesicles. Nat Rev Mol Cell Biol. 2018;19(4):213-28.
6. Yanez-Mo M, Siljander PR, Andreu Z, Zavec AB, Borras FE, Buzas EI, et al. Biological properties of extracellular vesicles and their physiological functions. Journal of extracellular vesicles. 2015;4:27066.
7. Krämer-Albers EM, Bretz N, Tenzer S, Winterstein C, Möbius W, Berger H, et al. Oligodendrocytes secrete exosomes containing major myelin and stress-protective proteins: Trophic support for axons? Proteomics Clinical applications. 2007;1(11):1446-61.
8. Frühbeis C, Fröhlich D, Kuo WP, Amphornrat J, Thilemann S, Saab AS, et al. Neurotransmitter-triggered transfer of exosomes mediates oligodendrocyte-neuron communication. PLoS biology. 2013;11(7):e1001604.
9. Fröhlich D, Kuo WP, Frühbeis C, Sun JJ, Zehendner CM, Luhmann HJ, et al. Multifaceted effects of oligodendroglial exosomes on neurons: impact on neuronal firing rate, signal transduction and gene regulation. Philosophical transactions of the Royal Society of London Series B, Biological sciences. 2014;369(1652).
10. Nave KA. Myelination and support of axonal integrity by glia. Nature. 2010;468(7321):244-52.
11. Griffiths I, Klugmann M, Anderson T, Yool D, Thomson C, Schwab MH, et al. Axonal swellings and degeneration in mice lacking the major proteolipid of myelin. Science. 1998;280(5369):1610-3.
12. Lappe-Siefke C, Goebbels S, Gravel M, Nicksch E, Lee J, Braun PE, et al. Disruption of Cnp1 uncouples oligodendroglial functions in axonal support and myelination. Nat Genet. 2003;33(3):366-74.
13. Edgar JM, McLaughlin M, Yool D, Zhang SC, Fowler JH, Montague P, et al. Oligodendroglial modulation of fast axonal transport in a mouse model of hereditary spastic paraplegia. The Journal of cell biology. 2004;166(1):121-31.
14. Fünfschilling U, Supplie LM, Mahad D, Boretius S, Saab AS, Edgar J, et al. Glycolytic oligodendrocytes maintain myelin and long-term axonal integrity. Nature. 2012;485(7399):517-21.
15. Lee Y, Morrison BM, Li Y, Lengacher S, Farah MH, Hoffman PN, et al. Oligodendroglia metabolically support axons and contribute to neurodegeneration. Nature. 2012;487(7408):443-8.
16. Saab AS, Tzvetanova ID, Nave KA. The role of myelin and oligodendrocytes in axonal energy metabolism. Curr Opin Neurobiol. 2013;23(6):1065-72.
17. Philips T, Rothstein JD. Oligodendroglia: metabolic supporters of neurons. J Clin Invest. 2017;127(9):3271-80.
18. Maday S, Twelvetrees AE, Moughamian AJ, Holzbaur EL. Axonal transport: cargo-specific mechanisms of motility and regulation. Neuron. 2014;84(2):292-309.
19. Morfini GA, Burns M, Binder LI, Kanaan NM, LaPointe N, Bosco DA, et al. Axonal transport defects in neurodegenerative diseases. J Neurosci. 2009;29(41):12776-86.
20. Sorbara CD, Wagner NE, Ladwig A, Nikic I, Merkler D, Kleele T, et al. Pervasive axonal transport deficits in multiple sclerosis models. Neuron. 2014;84(6):1183-90.
21. van den Berg R, Hoogenraad CC, Hintzen RQ. Axonal transport deficits in multiple sclerosis: spiraling into the abyss. Acta Neuropathol. 2017;134(1):1-14.
22. Kwinter DM, Lo K, Mafi P, Silverman MA. Dynactin regulates bidirectional transport of dense-core vesicles in the axon and dendrites of cultured hippocampal neurons. Neuroscience. 2009;162(4):1001-10.

23. Thery C, Witwer KW, Aikawa E, Alcaraz MJ, Anderson JD, Andriantsitohaina R, et al. Minimal information for studies of extracellular vesicles 2018 (MISEV2018): a position statement of the International Society for Extracellular Vesicles and update of the MISEV2014 guidelines. Journal of extracellular vesicles. 2018;7(1):1535750.
24. Frühbeis C, Fröhlich D, Kuo WP, Krämer-Albers EM. Extracellular vesicles as mediators of neuron-glia communication. Frontiers in cellular neuroscience. 2013;7:182.
25. Barnham KJ, Masters CL, Bush AI. Neurodegenerative diseases and oxidative stress. Nat Rev Drug Discov. 2004;3(3):205-14.
26. Holm MM, Kaiser J, Schwab ME. Extracellular Vesicles: Multimodal Envoys in Neural Maintenance and Repair. Trends Neurosci. 2018;41(6):360-72.
27. Raposo G, Stahl PD. Extracellular vesicles: a new communication paradigm? Nat Rev Mol Cell Biol. 2019;20(9):509-10.
28. Cantuti Castelvetri L, Givogri MI, Hebert A, Smith B, Song Y, Kaminska A, et al. The sphingolipid psychosine inhibits fast axonal transport in Krabbe disease by activation of GSK3beta and deregulation of molecular motors. J Neurosci. 2013;33(24):10048-56.
29. Nave KA. Myelination and the trophic support of long axons. Nat Rev Neurosci. 2010;11(4):275-83.
30. Stassart RM, Mobius W, Nave KA, Edgar JM. The Axon-Myelin Unit in Development and Degenerative Disease. Front Neurosci. 2018;12:467.
31. Snaidero N, Velte C, Myllykoski M, Raasakka A, Ignatev A, Werner HB, et al. Antagonistic Functions of MBP and CNP Establish Cytosolic Channels in CNS Myelin. Cell Rep. 2017;18(2):314-23.
32. Simons M, Krämer EM, Thiele C, Stoffel W, Trotter J. Assembly of myelin by association of proteolipid protein with cholesterol- and galactosylceramide-rich membrane domains. The Journal of cell biology. 2000;151(1):143-54.
33. Triplett JC, Zhang Z, Sultana R, Cai J, Klein JB, Bueler H, et al. Quantitative expression proteomics and phosphoproteomics profile of brain from PINK1 knockout mice: insights into mechanisms of familial Parkinson's disease. J Neurochem. 2015;133(5):750-65.
34. Kang CB, Hong Y, Dhe-Paganon S, Yoon HS. FKBP family proteins: immunophilins with versatile biological functions. Neurosignals. 2008;16(4):318-25.
35. Tytell M, Lasek RJ, Gainer H. Axonal maintenance, glia, exosomes, and heat shock proteins. F1000Res. 2016;5.
36. Xu J, Wang Y, Hsu CY, Gao Y, Meyers CA, Chang L, et al. Human perivascular stem cell-derived extracellular vesicles mediate bone repair. Elife. 2019;8.
37. Sleigh JN, Rossor AM, Fellows AD, Tosolini AP, Schiavo G. Axonal transport and neurological disease. Nat Rev Neurol. 2019.
38. Sommer I, Schachner M. Monoclonal antibodies (O1 to O4) to oligodendrocyte cell surfaces: an immunocytological study in the central nervous system. Dev Biol. 1981;83(2):311-27.
39. Klugmann M, Schwab MH, Puhlhofer A, Schneider A, Zimmermann F, Griffiths IR, et al. Assembly of CNS myelin in the absence of proteolipid protein. Neuron. 1997;18(1):59-70.
40. Krämer EM, Koch T, Niehaus A, Trotter J. Oligodendrocytes direct glycosyl phosphatidylinositol-anchored proteins to the myelin sheath in glycosphingolipid-rich complexes. J Biol Chem. 1997;272(14):8937-45.
41. Feldmann A, Amphornrat J, Schonherr M, Winterstein C, Mobius W, Ruhwedel T, et al. Transport of the major myelin proteolipid protein is directed by VAMP3 and VAMP7. J Neurosci. 2011;31(15):5659-72.
42. Klugmann M, Symes CW, Leichtlein CB, Klaussner BK, Dunning J, Fong D, et al. AAV-mediated hippocampal expression of short and long Homer 1 proteins differentially affect cognition and seizure activity in adult rats. Molecular and cellular neurosciences. 2005;28(2):347-60.
43. Distler U, Kuharev J, Navarro P, Levin Y, Schild H, Tenzer S. Drift time-specific collision energies enable deep-coverage data-independent acquisition proteomics. Nat Methods. 2014;11(2):167-70.

Acknowledgements

We thank Lilja Niedens for technical help and Sandra Ritz for providing expertise on live cell imaging and image analysis. We are grateful to A. Andrieux for hosting WPKE in her laboratory and for valuable discussion. WPKE was supported by a stipend of the Focus Programme of Translational Neuroscience. The study was funded by JGU Mainz intramural funding and by DFG grants KR 3668/1-1 and KR 3668/1-2 to EMKA. KAN is supported by an ERC Advanced Grant (MyeliNANO) and the Adelson Medical Research Foundation.

Author Contributions

CF, WPKE, KM, DF, LP, EMKA conceived and designed experiments. CF, WPKE, KM, DM, ST, WM performed experiments. KAN and HW provided materials. CF, WPKE, KM, DF, ST, and EMKA collected and analysed data. CF, WPKE, EMKA wrote the manuscript.

Competing interests

None

Figure legends

Figure 1. Influence of oligodendroglial sEVs on axonal transport under resting conditions. (**A**) Illustration of experimental schedule. sEVs were applied to hippocampal neurons and imaged after 30 min. (**B**) Representative kymographs and corresponding time-lapse frames illustrating movement of BDNF-mCherry positive vesicles (arrow) along the axon of primary hippocampal neurons. Neurons were sham treated (control) or treated with oligodendroglial sEVs (OL sEVs). (**C-E**) Quantitative analysis of kymographs considering total movement (**C**), velocity (**D**), and pausing time (**E**) of BDNF-mCherry-positive vesicles. Error bars depict SEM, n=12 recorded neurons from 3 independent experiments, ***p<0.0001, two-tailed Student's t-test with Holm-Sidak correction.

Figure 2. Influence of sEVs on axonal transport under oxidative stress. (**A**) Illustration of experimental schedule. Hippocampal neurons were pretreated with sEVs before exposure to oxidative stress (OS) and live imaging. (**B**) Representative kymographs and corresponding time-lapse frames illustrating movement of BDNF-mCherry positive vesicles (arrow) generated from hippocampal neurons sham-treated or treated with sEVs derived from oligodendrocytes (OL) or HEK293T cells. (**C-E**) Quantitative analysis of kymographs regarding total movement (**C**), velocity (**D**), and pausing time (**E**) of BDNF-mCherry-positive vesicles. Error bars depict SEM, n=13 for untreated and OL-sEV treated neurons and n=7 for HEK-sEV treated neurons derived from 3 independent experiments, *p<0.05, ***p<0.001, two-tailed Student's t-test with Holm-Sidak correction.

Figure 3: Influence of sEVs on axonal transport under starvation stress. (**A**) Illustration of experimental schedule. Hippocampal neurons were treated with sEVs and subjected to starvation stress by nutrient deprivation (ND) during the last 3 hours before live imaging. (**B**) Representative kymographs and corresponding time-lapse frames illustrating movement of BDNF-mCherry positive vesicles (arrow) generated from hippocampal neurons exposed to ND. Neurons were kept in complete medium (unstressed) or subjected to nutrient-deprivation in absence (ND) or presence of sEVs (ND + OL sEVs). (**C-E**) Quantitative analysis of kymographs regarding total movement (**C**), velocity (**D**), and pausing time (**E**) of BDNF-mCherry-positive vesicles. Error bars depict SEM, n=21 recorded neurons from 3 independent experiments, *p<0.05, **p<0.01, ***p<0.001, two-tailed Student's t-test with Holm-Sidak correction.

Figure 4: Impaired exosome release from PLP- and CNP-null oligodendrocytes. (**A**) Representative electron microscopy images taken from optic nerve cross sections

demonstrating MVBs (arrows) in different oligodendrocyte compartments (from left to right): in the inner cytoplasmic loop close to the axon (adaxonal), in cytoplasmic channels within myelin (myelin), in outer cytoplasmic loop (abaxonal), or in oligodendrocyte cell bodies (scale bar 500 nm). (**B-D**) Quantification of oligodendrocyte MVBs counted in optic nerves of wild type (WT), CNP- and PLP-null (CNPko, PLPko) animals and depicted as (**B**), overall number of MVBs per axon or (**C, D**), relative number of MVBs located in different compartments as indicated in A. SEM, n=3. **(E**) Nanoparticle tracking analysis of sEVs isolated from WT, CNP-, and PLP-null oligodendrocytes normalized to the number of secreting cells. SEM, n=3. (**F**) Representative Western blot of isolated sEVs derived from equal numbers of WT, CNP-, and PLP-null oligodendrocytes and (**G**) densiometric quantification. Signals from sEVs were normalized to the total cell lysate of corresponding sEV secreting cells and expressed in relation to wild-type levels (dashed line). SEM, n=2-5.

Figure 5: Differential proteome analysis of wild-type PLP- and CNP-null exosomes. LC-MS analysis of density-gradient-purified sEVs. (**A**) Functional annotation to Gene Ontology terms “cellular component” and “biological process”. (**B**) Volcano Blot of proteins over- or underrepresented in null-mutant (PLPko, CNPko) versus wild-type (WT) sEVs. Proteins downregulated in both PLPko and CNPko sEVs are labelled in red. (**C**) Venn diagram illustrating overlap of up- and downregulated proteins between PLPko and CNPko sEVs. (**D**) List of top10 downregulated proteins in PLPko and CNPko sEVs and their level of downregulation expressed as log2 fold change (underlined by green colour intensity). PLP and CNP are at top of list due to genetic deletion (highlighted in grey). Proteins underrepresented in both PLPko and CNPko are highlighted in red. (**E**) Western blot analysis of sEVs isolated from WT, CNPko, and PLPko oligodendrocytes normalized to particle number and (**F**) densitometric quantification (n=2-4). Protein levels are expressed relative to wild-type (dashed line).

Figure 6: PLP- and CNP-null exosomes deliver cargo but lack functional activity. (**A**) Western blot showing hrGFP reporter gene activation in primary cortical neurons (CN) upon exposure to Cre-labelled oligodendroglial (OL) sEVs secreted from equal numbers of wild-type (WT), CNP-null (CNPko), or PLP-null (PLPko) oligodendrocytes. Control shows background in neurons not receiving Cre-sEVs. Alpha-tubulin, loading control. (**B**) Quantitative representation of hrGFP Western blot signals normalized to alpha-tubulin and expressed relative to wild-type signal (dashed line). SEM, n=4-5, ANOVA followed by Dunn’s multiple comparison test, *p<0.05, **p<0,001. (**C**) Dose response curve of sEV-mediated protection of cortical neurons from nutrient-deprivation (ND). Metabolic activity was measured in neurons receiving a series of dilutions of sEV-containing supernatants derived from wild-type oligodendrocytes (100 % =

undiluted 10K supernatants, 0 % = sEV-deprived 100K supernatants). Dashed line, reference of unstarved neurons (n=5, SEM), one-way ANOVA test with Dunn's multiple comparison test, *p<0.05, **p<0,001. (**D, E**) Metabolic activity of cortical neurons subjected to nutrient-deprivation (ND, sham) treated with sEV-containing 10K supernatants (+OL sEV) derived from wild-type (WT), CNP-null (CNPko), or PLP-null (PLPko) oligodendrocytes. Grey bar compares treatment with sEV-depleted 100K supernatants (-OL sEV) derived from wild-type (WT) oligodendrocytes. Dashed line, reference of unstarved neurons. (**D**) sEV input was normalized to according the number of sEV-secreting cells (n=3-5, SEM) or (**E**) to the number of particles applied to neurons, as determined by NTA (n=3-6), two-tailed Student's t-test, *p<0.05, **p<0,001, ***p<0,0001.

Figure 7: PLP- and CNP-null exosomes do not promote axonal transport under starvation stress. (**A**) Illustration of experimental schedule. Hippocampal neurons were treated with sEVs and subjected to starvation stress by nutrient deprivation (ND) during the last 3 hours before live imaging. (**B**) Representative kymographs and corresponding time-lapse frames illustrating movement of BDNF-mCherry positive vesicles (arrow) generated from hippocampal neurons exposed to nutrient deprivation ND and treated with sEVs derived from wild-type (WT), CNPko, PLPko oligodendroytes or primary astrocytes (Astro). (**C-E**) Quantitative analysis of kymographs regarding total movement (**C**), velocity (**D**), and pausing time (**E**) of BDNF-mCherry-positive vesicles. Error bars depict SEM; n=21 recorded neurons for control, ND+WT sEVs, and ND+PLPko sEVs; n=25 for ND+CNPko sEVs; n=20 for ND; n=7 for ND+astro sEVs, derived from 3 independent experiments, *p<0.05, **p<0.01, ***p<0.001, two-tailed Student's t-test with Holm-Sidak correction. Significance only indicated for wild-type versus mutant sEVs for reasons of clarity (see Fig. 3 for wild-type significance).

Figure 1

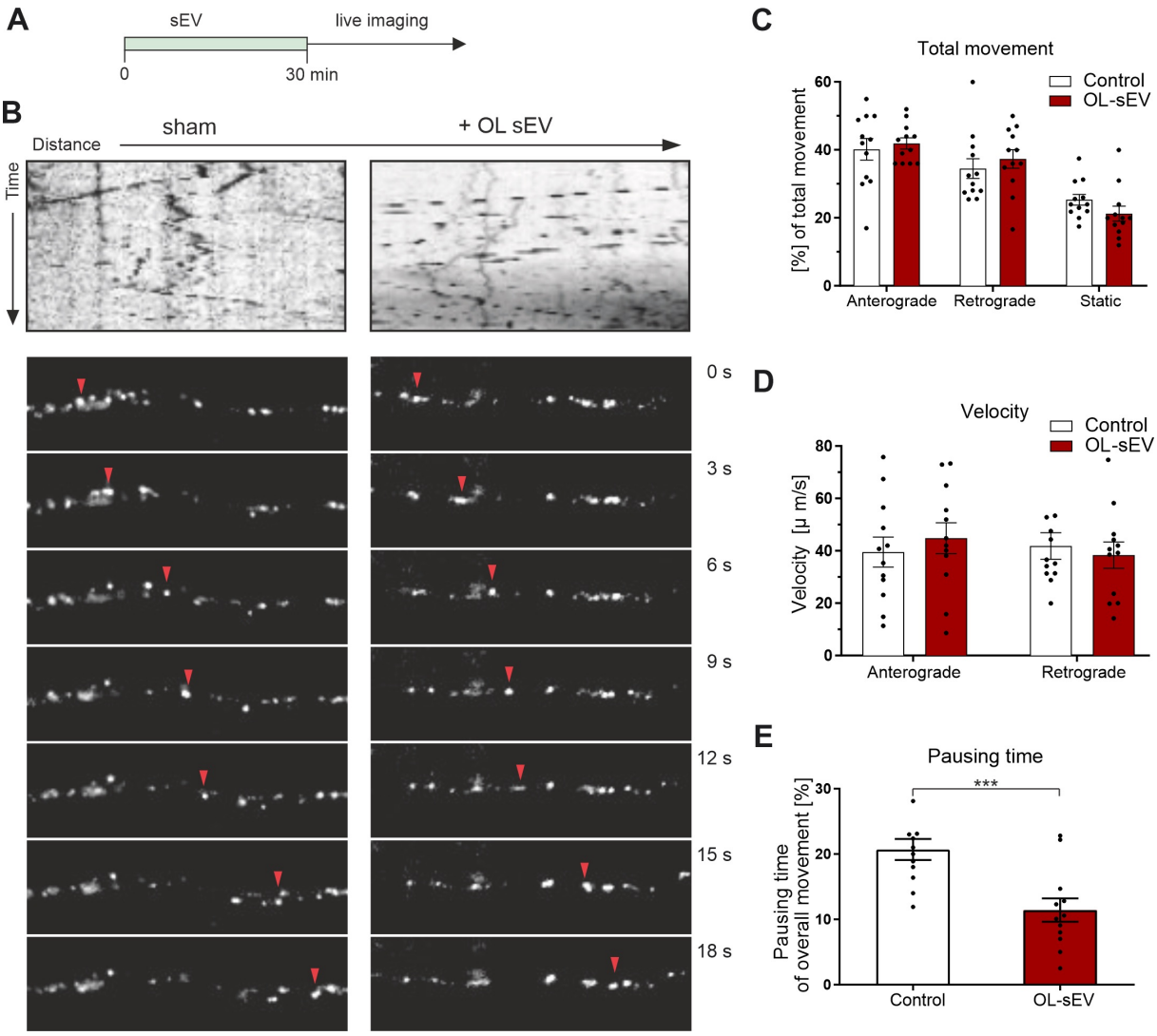

Figure 2

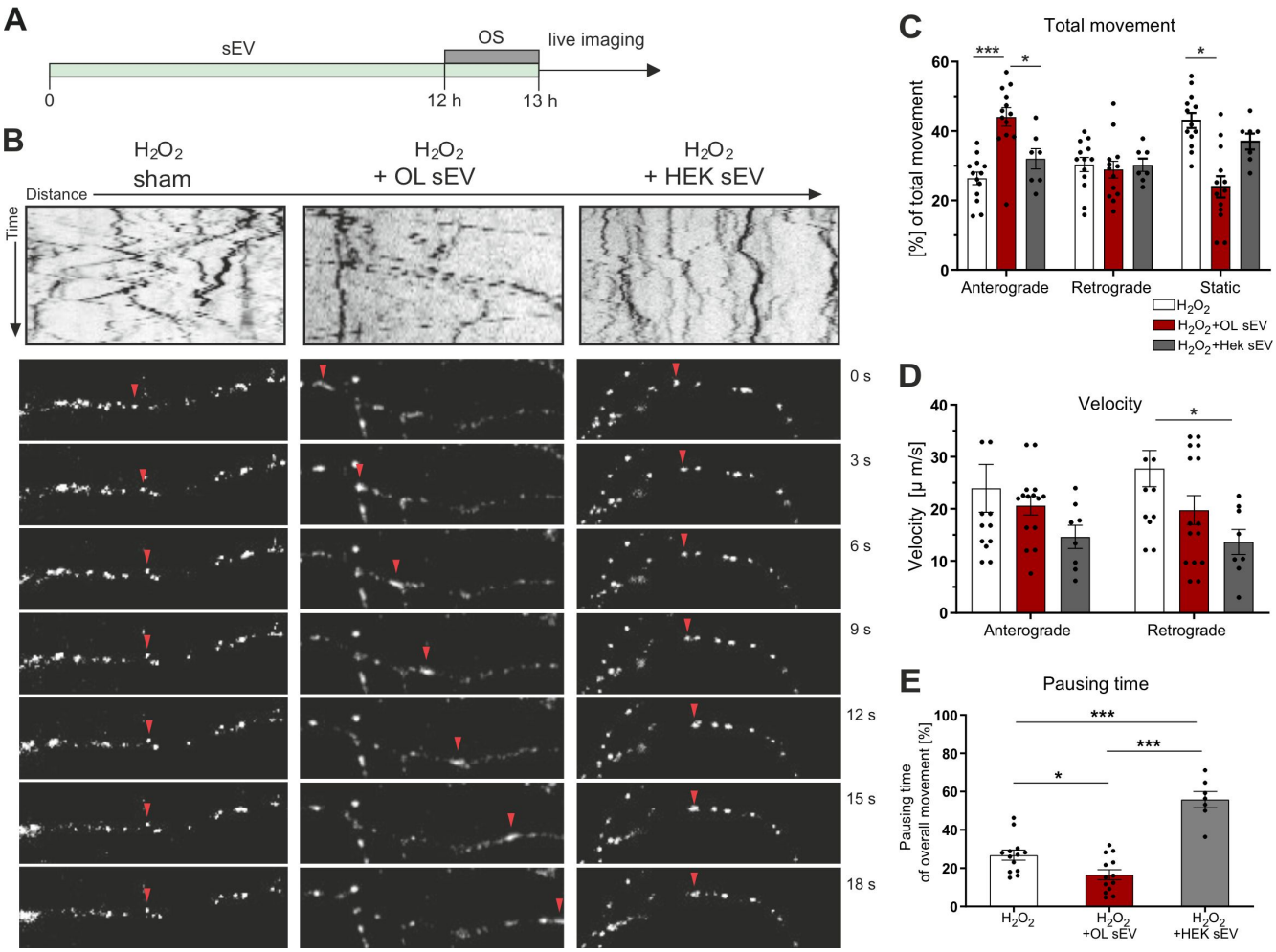

Figure 3

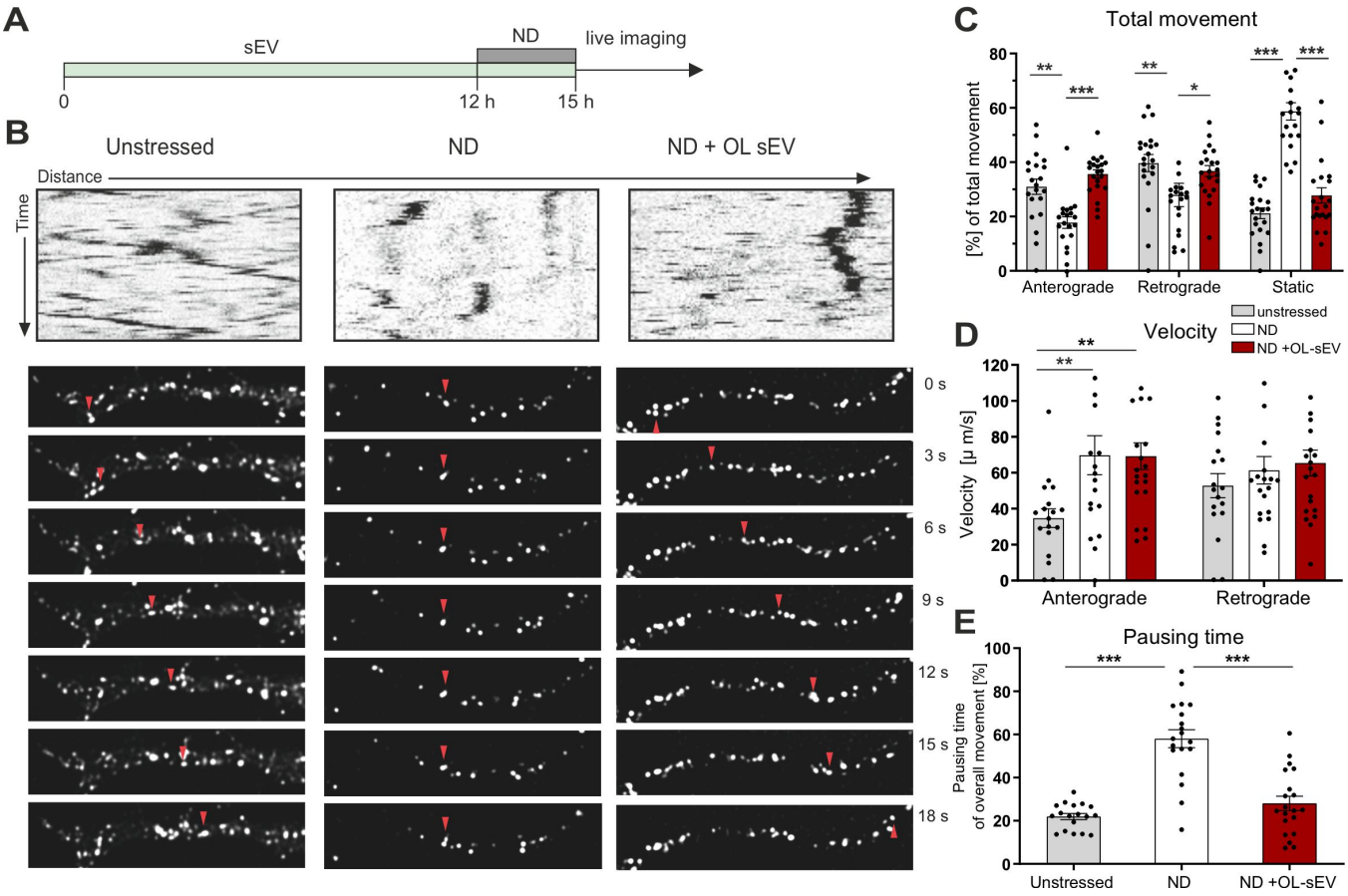

Figure 4

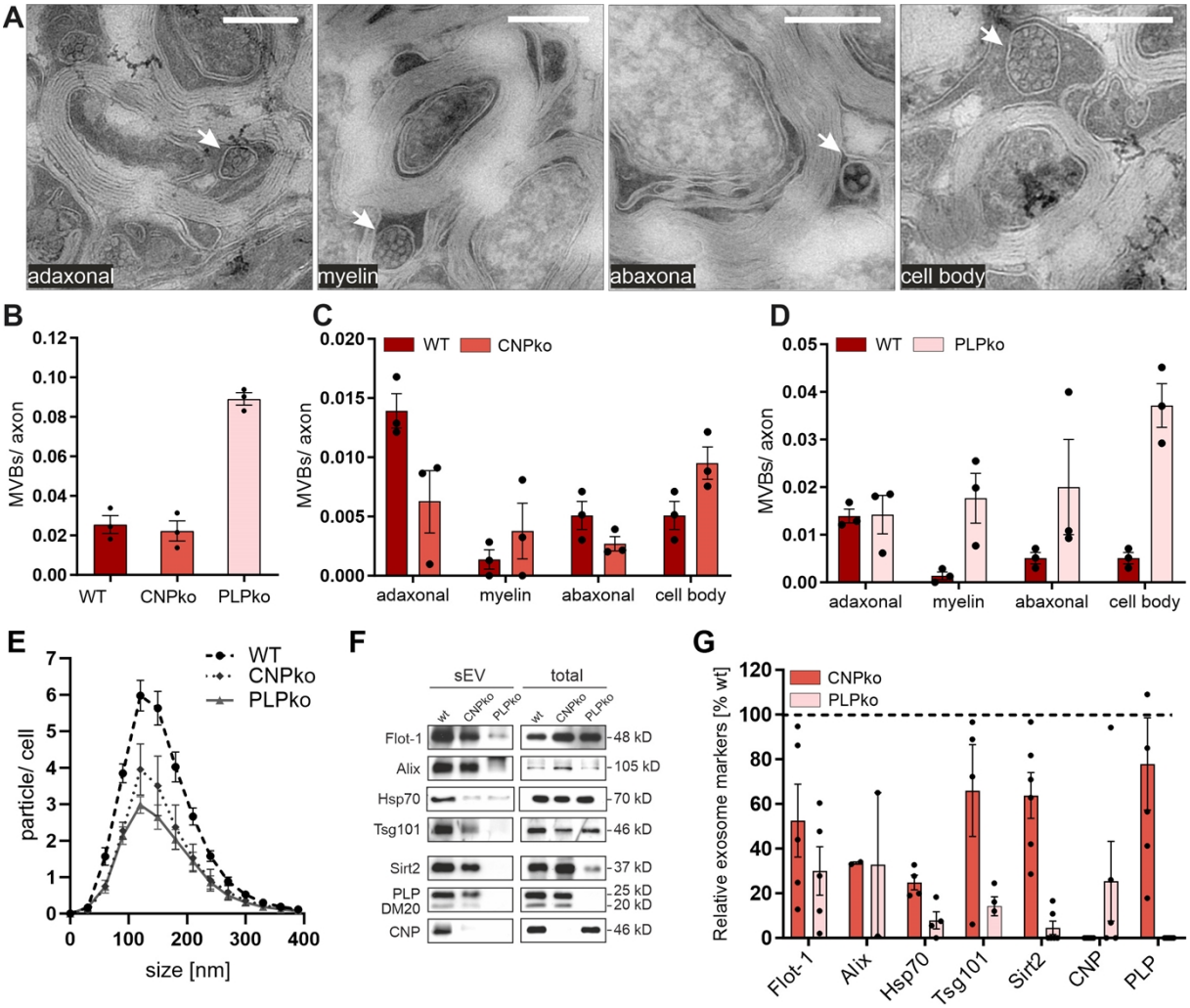

Figure 5

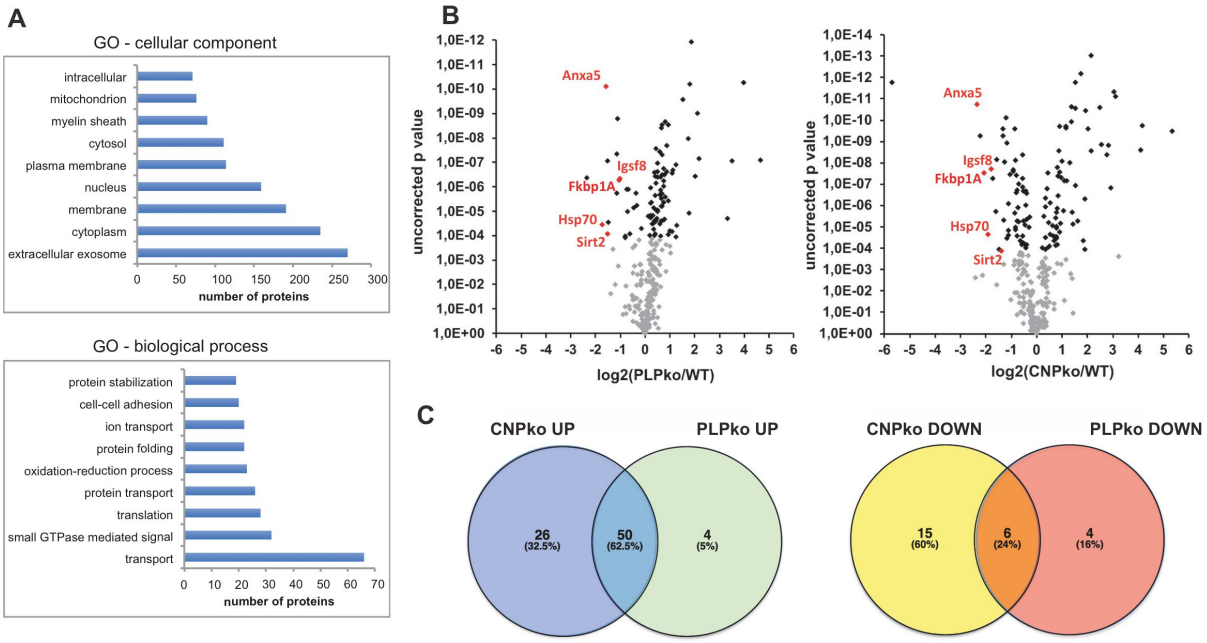

D

Top 10 down CNPko versus wt		
description	entry	log2Ratio
2',3'-cyclic-nucleotide 3'-phosphodiesterase	CN37_MOUSE	-5,69
G(i) subunit alpha-1	GNAI1_MOUSE	-5,78
Annexin A5	ANXA5_MOUSE	-2,32
Carbonic anhydrase 2	CAH2_MOUSE	-2,20
Peptidyl-prolyl cis-trans isomerase	FKB1A_MOUSE	-2,07
Heat shock-related 70 kDa	HSP72_MOUSE	-1,89
Immunoglobulin superfamily member 8	IGSF8_MOUSE	-1,78
Cystatin-B	CYTB_MOUSE	-1,59
Sirtuin-2	SIR2_MOUSE	-1,36
Gelsolin	GELS_MOUSE	-1,31
Dihydropyrimidinase-related protein 2	DPYL2_MOUSE	-1,31

Top 10 down PLPko versus wt		
description	entry	log2Ratio
Myelin proteolipid protein	MYPR_MOUSE	-10,42
Heat shock-related 70 kDa protein 2	HSP72_MOUSE	-1,73
Annexin A5	ANXA5_MOUSE	-1,57
Sirtuin-2	SIR2_MOUSE	-1,49
Serotransferrin	TRFE_MOUSE	-1,48
Endoplasmin	ENPL_MOUSE	-1,11
Clathrin heavy chain 1	CLH_MOUSE	-1,09
Peptidyl-prolyl cis-trans isomerase	FKB1A_MOUSE	-1,03
Immunoglobulin superfamily member 8	IGSF8_MOUSE	-1,00
Myelin-associated glycoprotein	MAG_MOUSE	-0,80
G(t) subunit alpha-3	GNAT3_MOUSE	-0,78

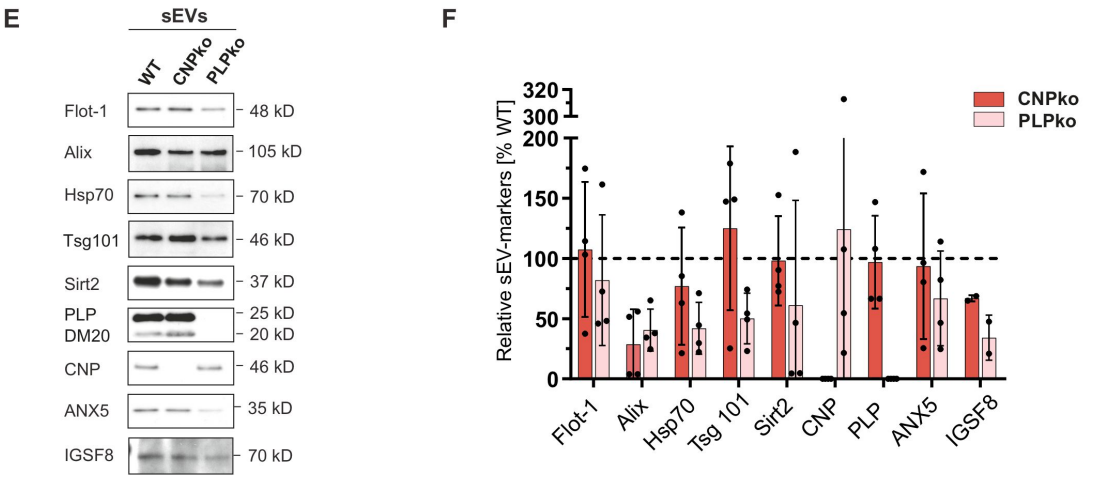

Figure 6

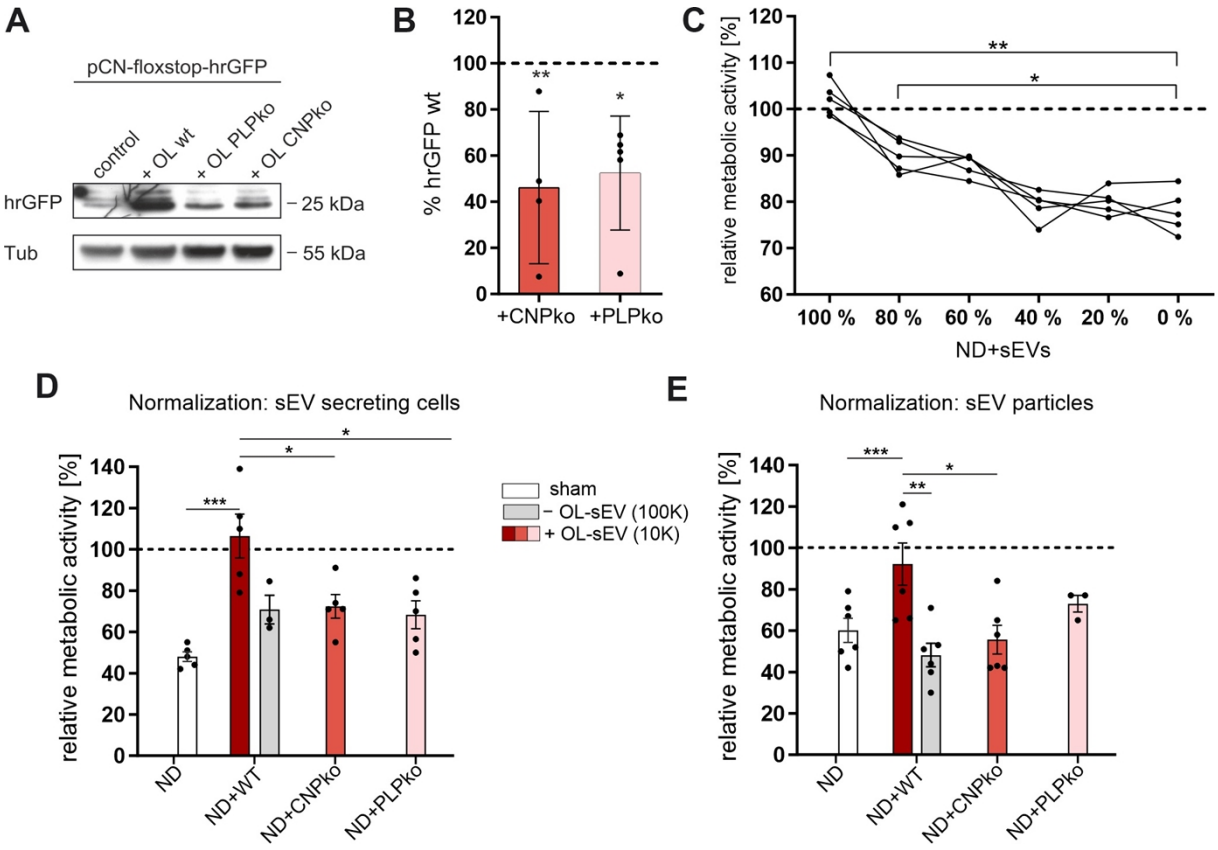

Figure 7

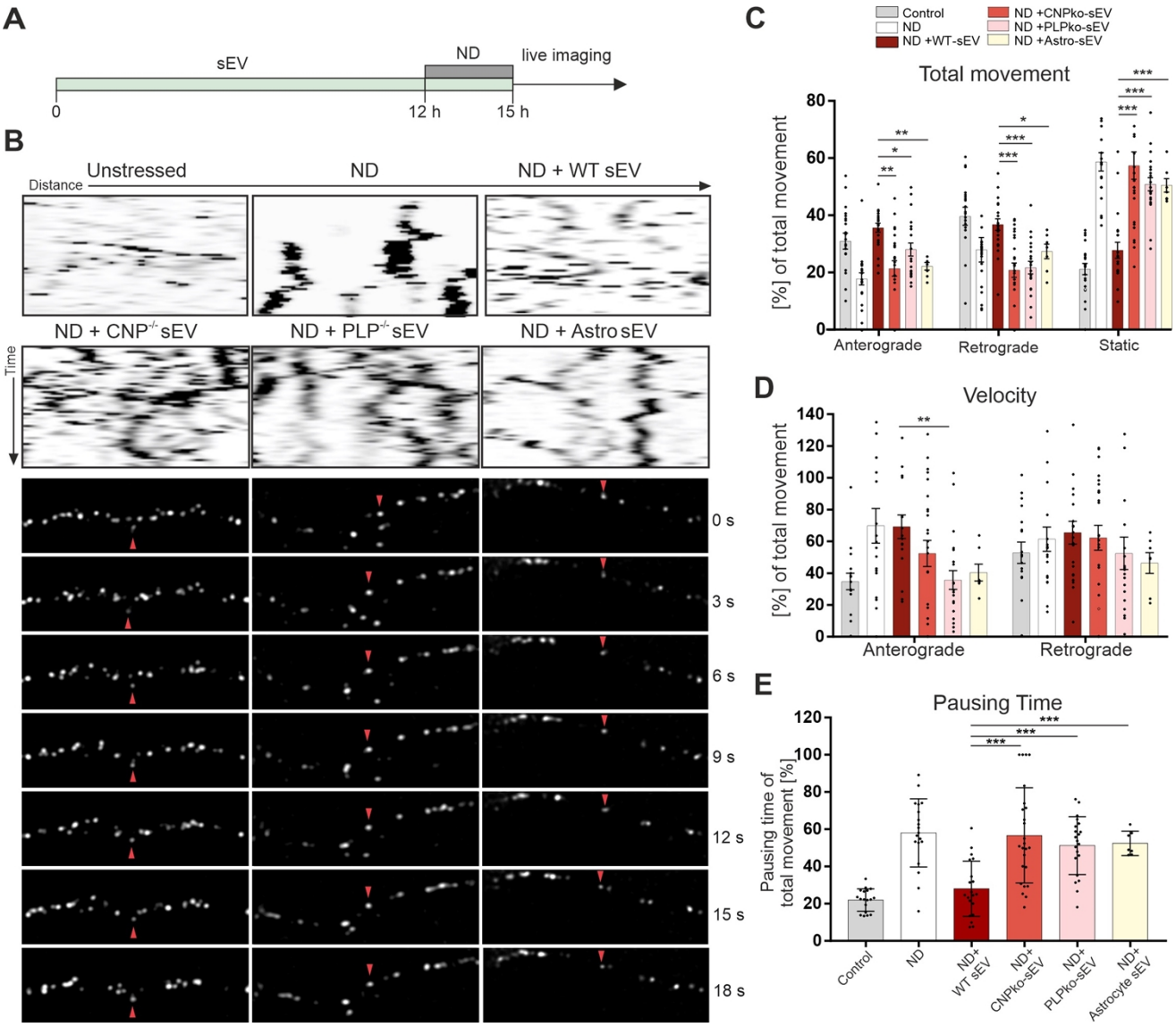

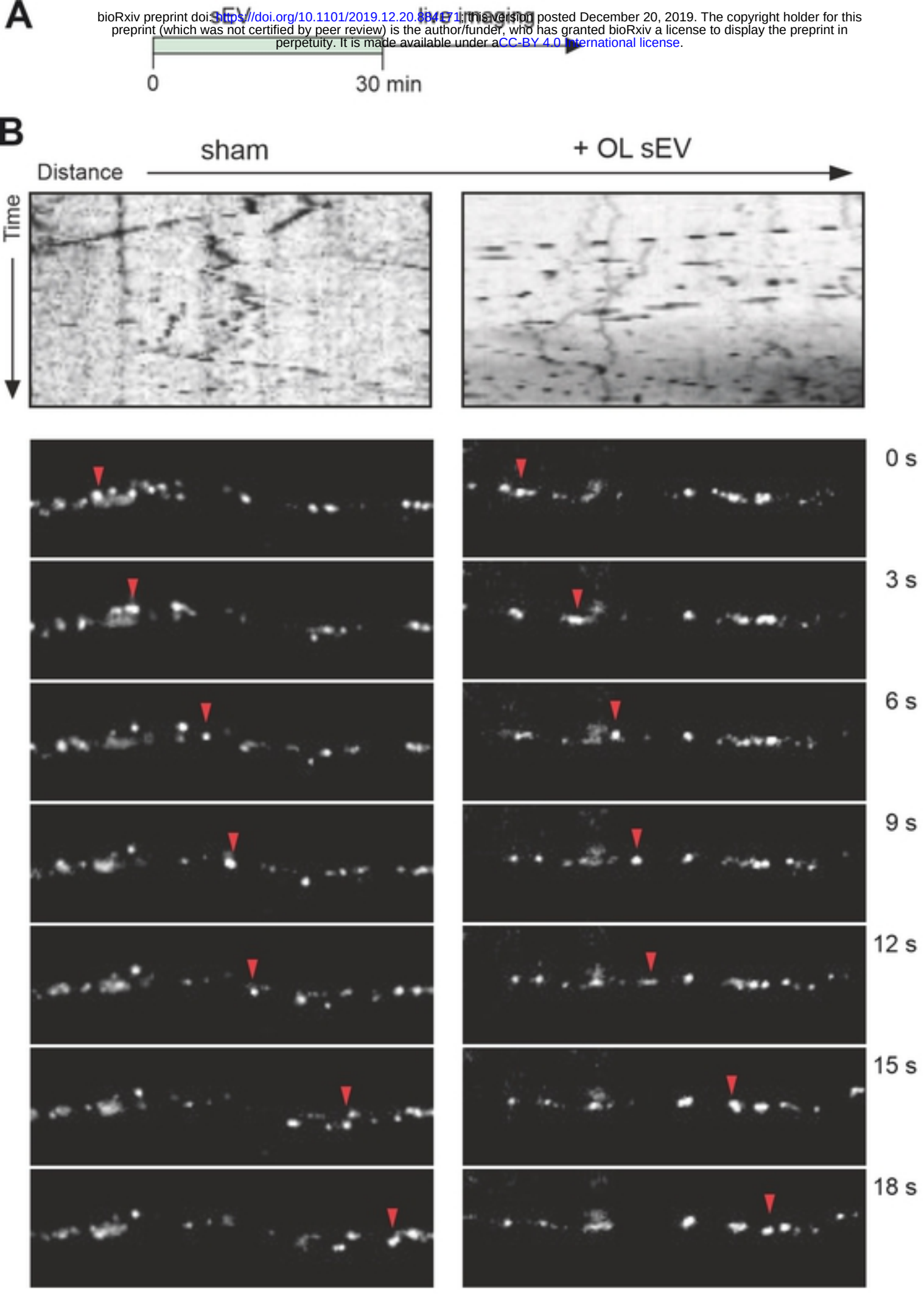

Figure 1

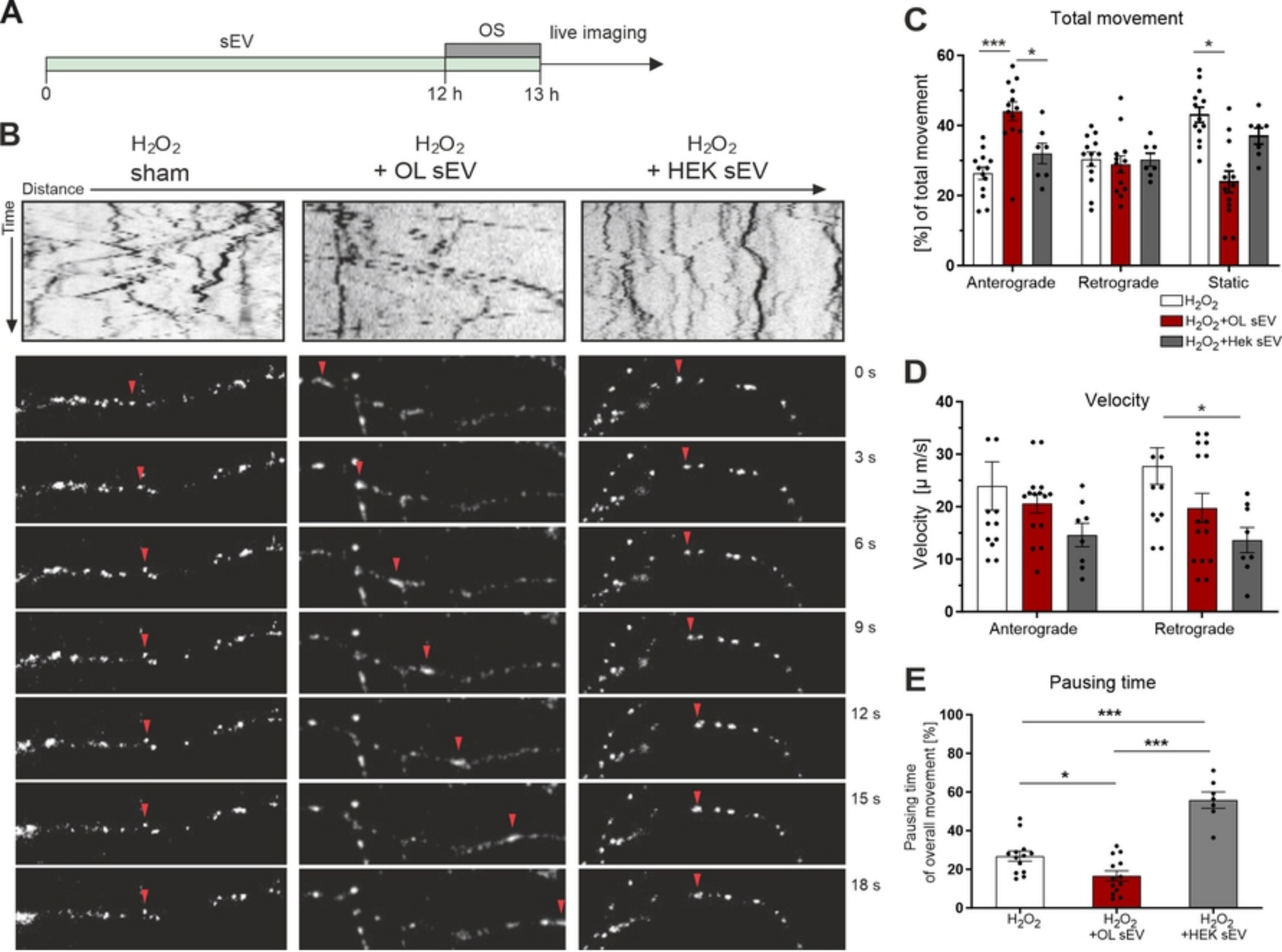
A
sEV
OS
live imaging
0
12 h
13 h
B
H2O2
sham
H2O2
+ OL sEV
H2O2
+ HEK sEV
Distance
Time
0 s
3 s
6 s
9 s
12 s
15 s
18 s
C
Total movement
[%] of total movement
Anterograde
Retrograde
Static
H2O2
H2O2+OL sEV
H2O2+Hek sEV
D
Velocity
Velocity [µ m/s]
Anterograde
Retrograde
E
Pausing time
Pausing time of overall movement [%]
H2O2
H2O2 +OL sEV
H2O2 +HEK sEV

Figure 2

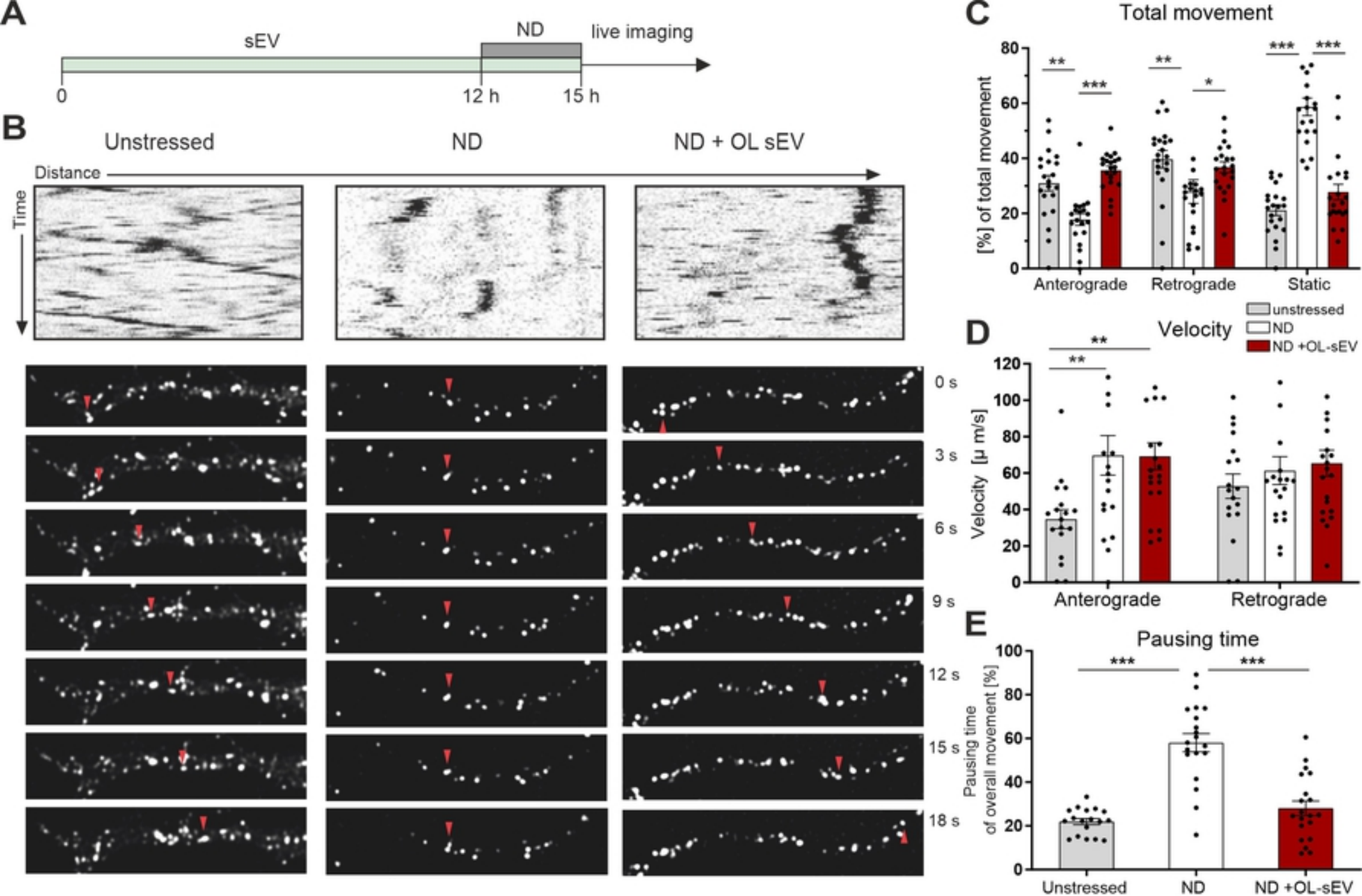
A
sEV
ND
live imaging
0
12 h
15 h
B
Unstressed
ND
ND + OL sEV
Distance
Time
0 s
3 s
6 s
9 s
12 s
15 s
18 s
C
Total movement
[%] of total movement
Anterograde
Retrograde
Static
unstressed
ND
ND +OL-sEV
D
Velocity
Velocity [µ m/s]
Anterograde
Retrograde
E
Pausing time
Pausing time of overall movement [%]
Unstressed
ND
ND +OL-sEV

Figure 3

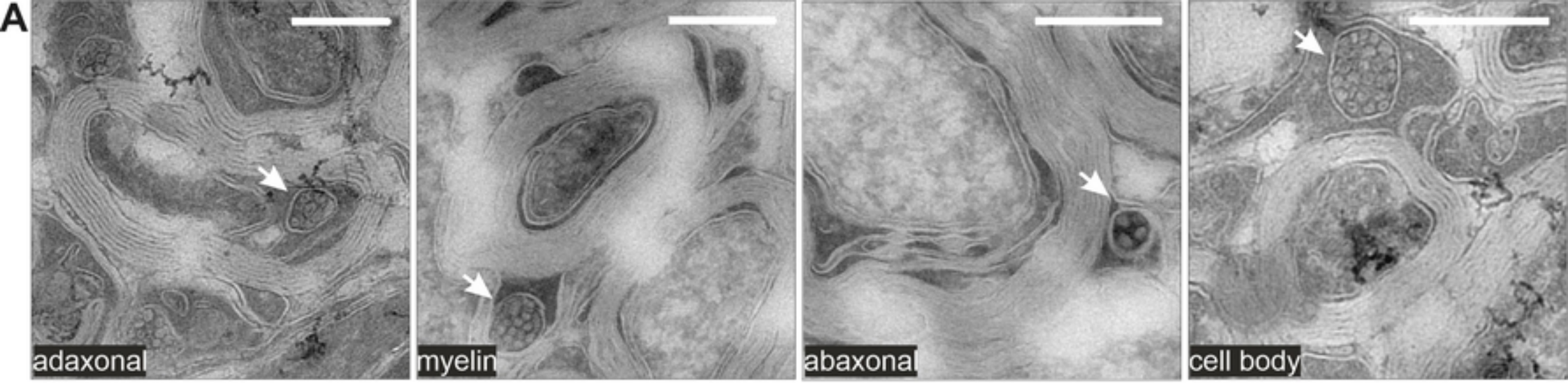
A
adaxonal
myelin
abaxonal
cell body

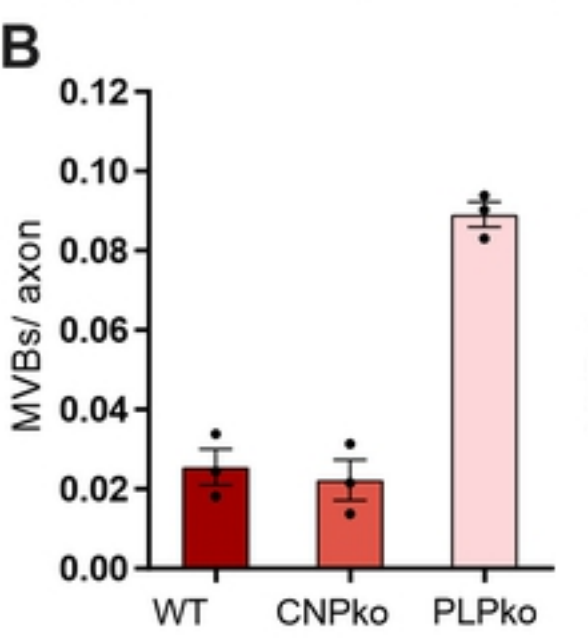
B
MVBs/ axon
0.12
0.10
0.08
0.06
0.04
0.02
0.00
WT
CNPko
PLPko

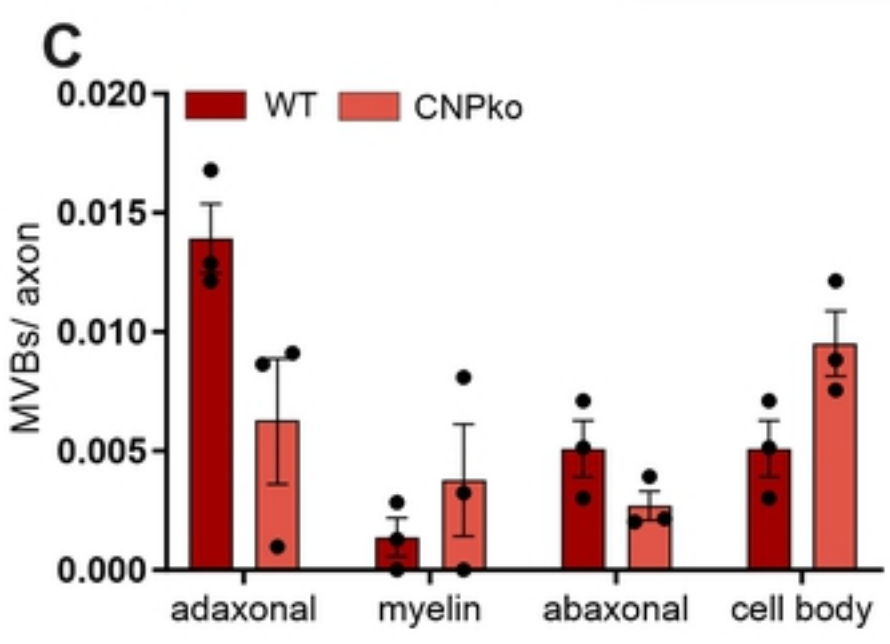
C
WT
CNPko
MVBs/ axon
0.020
0.015
0.010
0.005
0.000
adaxonal
myelin
abaxonal
cell body

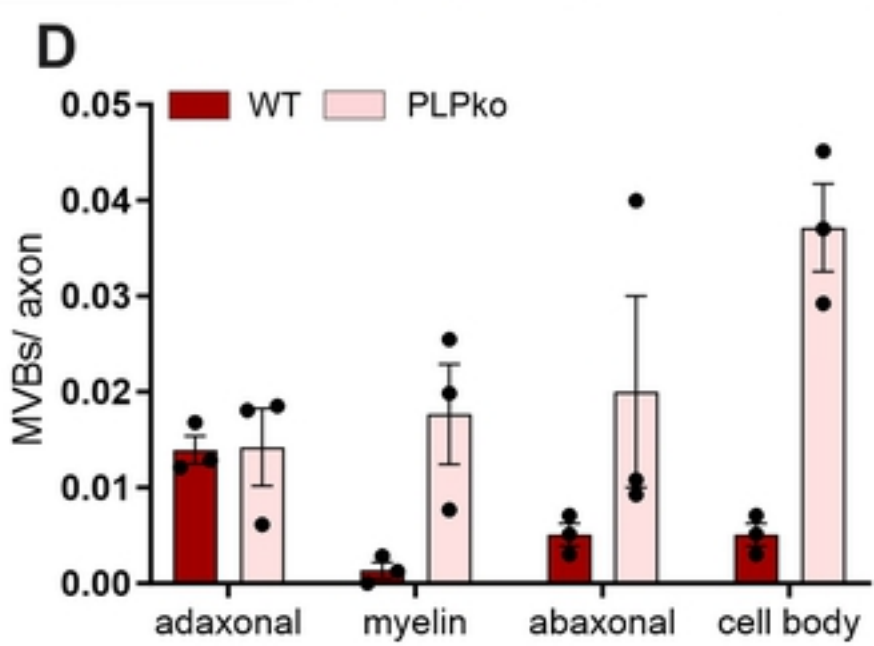
D
WT
PLPko
MVBs/ axon
0.05
0.04
0.03
0.02
0.01
0.00
adaxonal
myelin
abaxonal
cell body

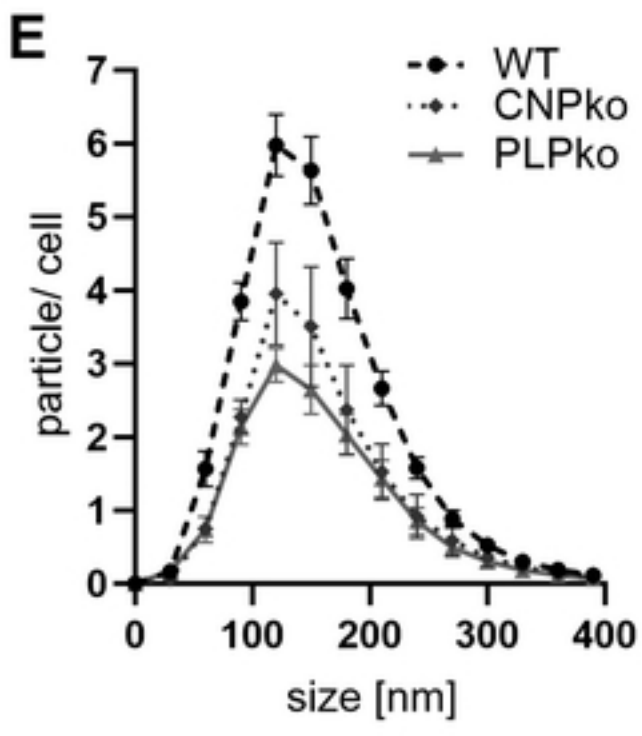
E
WT
CNPko
PLPko
particle/ cell
7
6
5
4
3
2
1
0
0
100
200
300
400
size [nm]

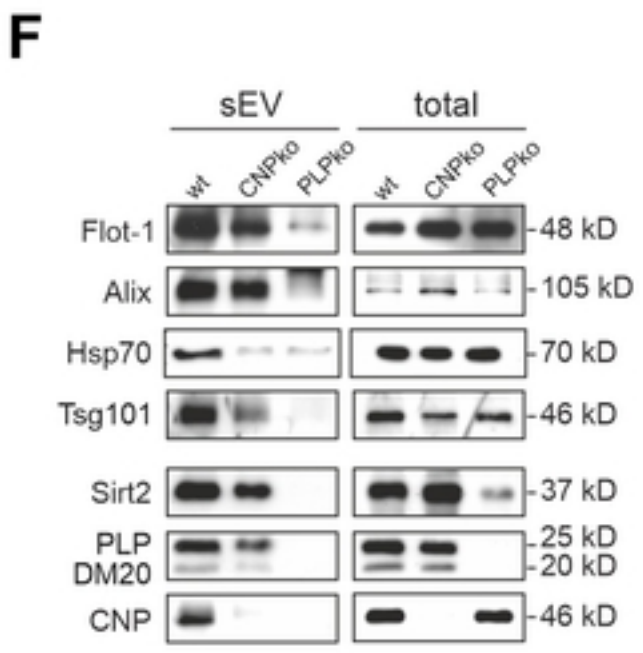
F
sEV
total
wt
CNPko
PLPko
Flot-1
Alix
Hsp70
Tsg101
Sirt2
PLP
DM20
CNP
48 kD
105 kD
70 kD
46 kD
37 kD
25 kD
20 kD
46 kD

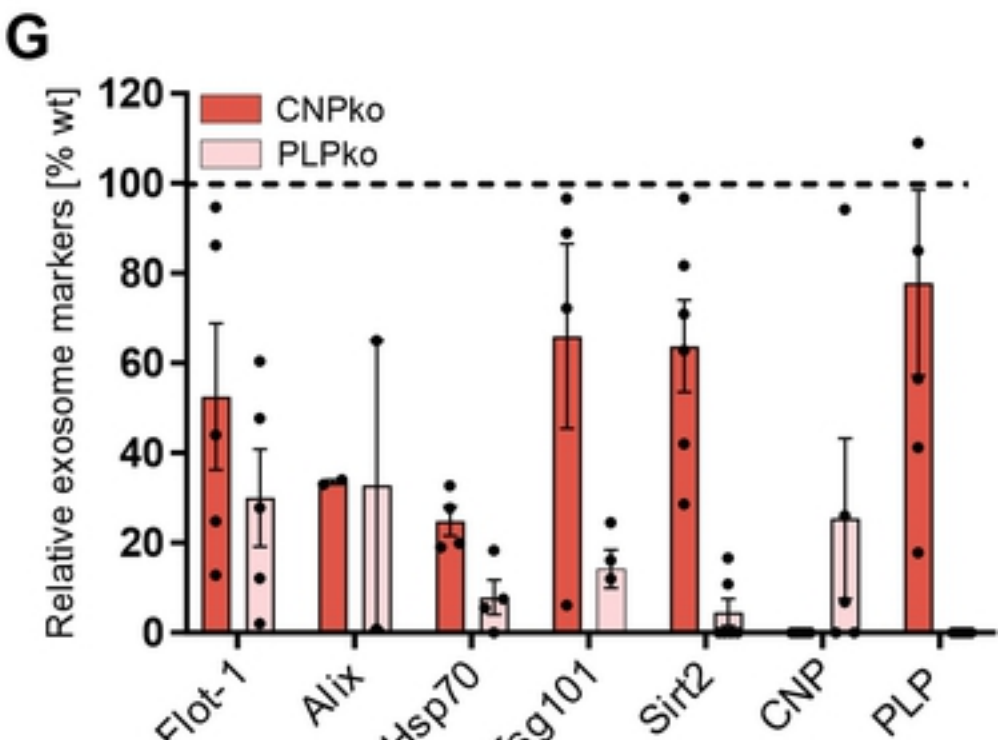
G
CNPko
PLPko
Relative exosome markers [% wt]
120
100
80
60
40
20
0
Flot-1
Alix
Hsp70
Tsg101
Sirt2
CNP
PLP

Figure 4

A

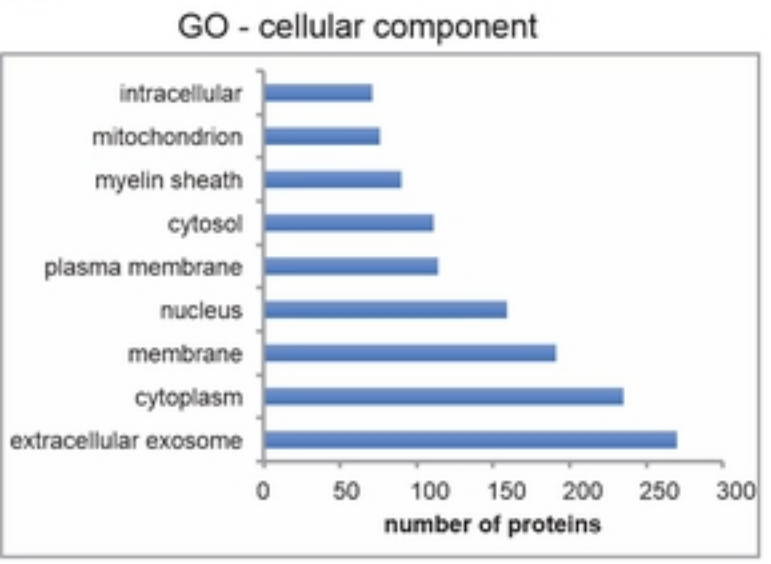

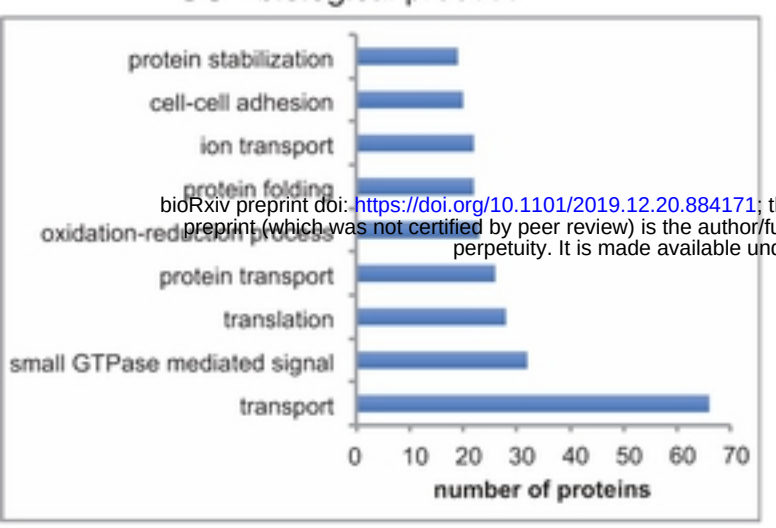

B

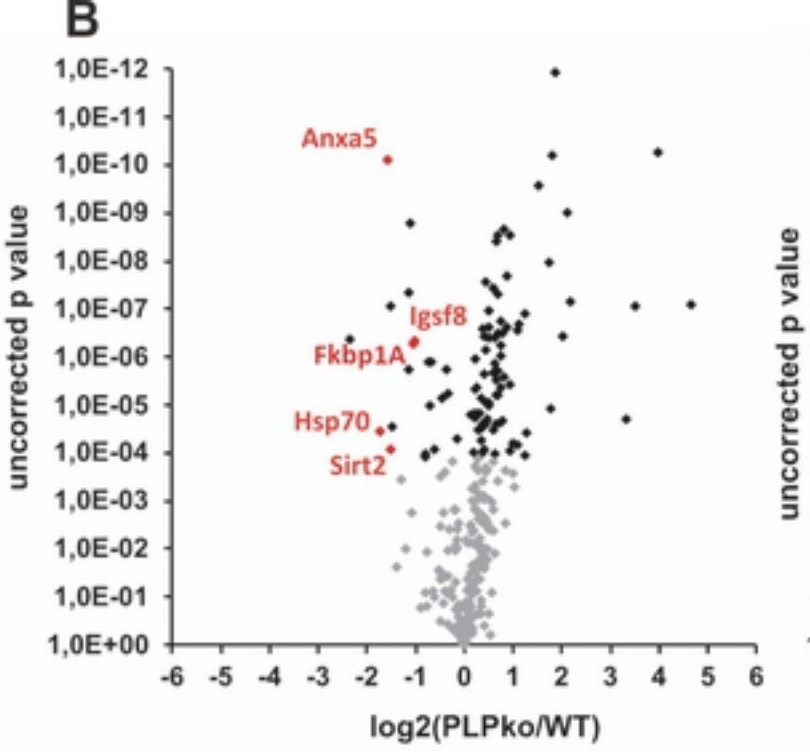

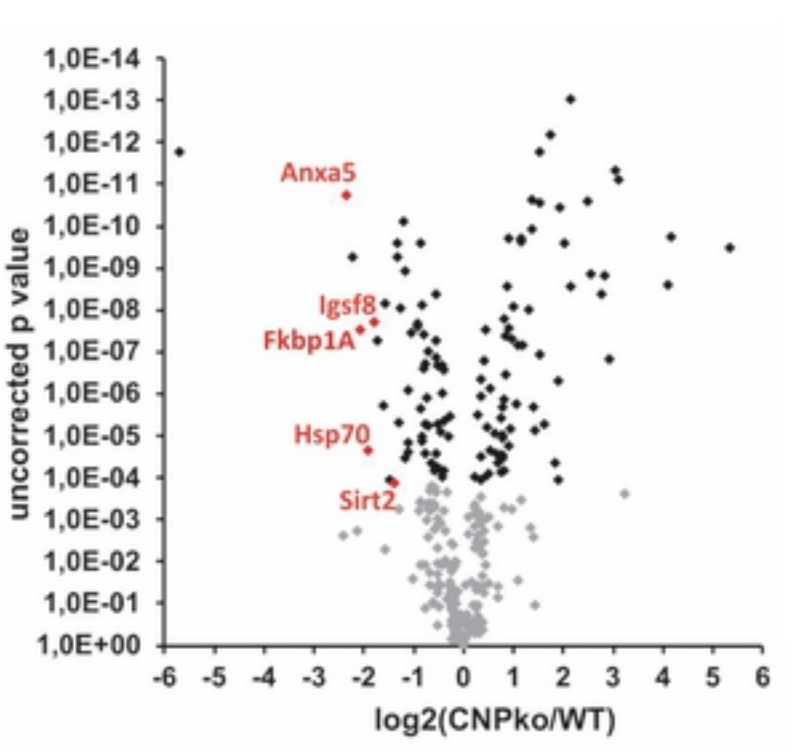

C

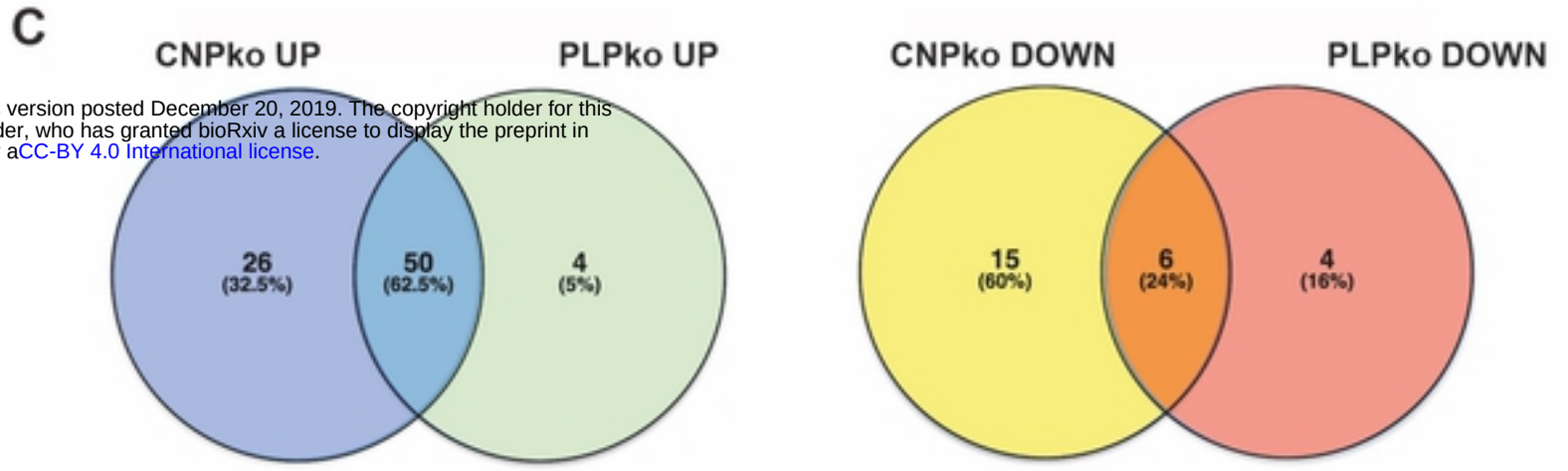

D

Top 10 down CNPko versus wt		
description	entry	log2Ratio
2',3'-cyclic-nucleotide 3'-phosphodiesterase	CN37_MOUSE	-5,69
G(i) subunit alpha-1	GNAI1_MOUSE	-5,78
Annexin A5	ANXA5_MOUSE	-2,32
Carbonic anhydrase 2	CAH2_MOUSE	-2,20
Peptidyl-prolyl cis-trans isomerase	FKB1A_MOUSE	-2,07
Heat shock-related 70 kDa	HSP72_MOUSE	-1,89
Immunoglobulin superfamily member 8	IGSF8_MOUSE	-1,78
Cystatin-B	CYTB_MOUSE	-1,59
Sirtuin-2	SIR2_MOUSE	-1,36
Gelsolin	GELS_MOUSE	-1,31
Dihydropyrimidinase-related protein 2	DPYL2_MOUSE	-1,31

Top 10 down PLPko versus wt		
description	entry	log2Ratio
Myelin proteolipid protein	MYPR_MOUSE	-10,42
Heat shock-related 70 kDa protein 2	HSP72_MOUSE	-1,73
Annexin A5	ANXA5_MOUSE	-1,57
Sirtuin-2	SIR2_MOUSE	-1,49
Serotransferrin	TRFE_MOUSE	-1,48
Endoplasmin	ENPL_MOUSE	-1,11
Clathrin heavy chain 1	CLH_MOUSE	-1,09
Peptidyl-prolyl cis-trans isomerase	FKB1A_MOUSE	-1,03
Immunoglobulin superfamily member 8	IGSF8_MOUSE	-1,00
Myelin-associated glycoprotein	MAG_MOUSE	-0,80
G(t) subunit alpha-3	GNAT3_MOUSE	-0,78

E

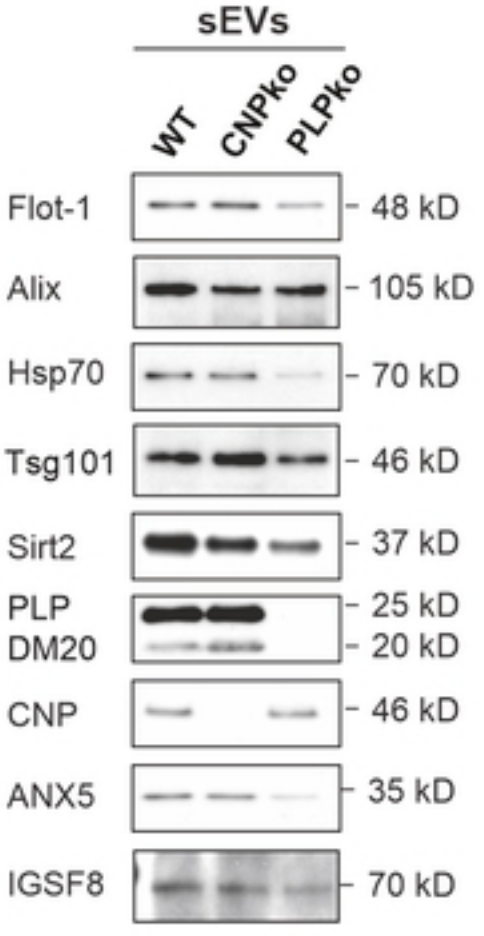

F

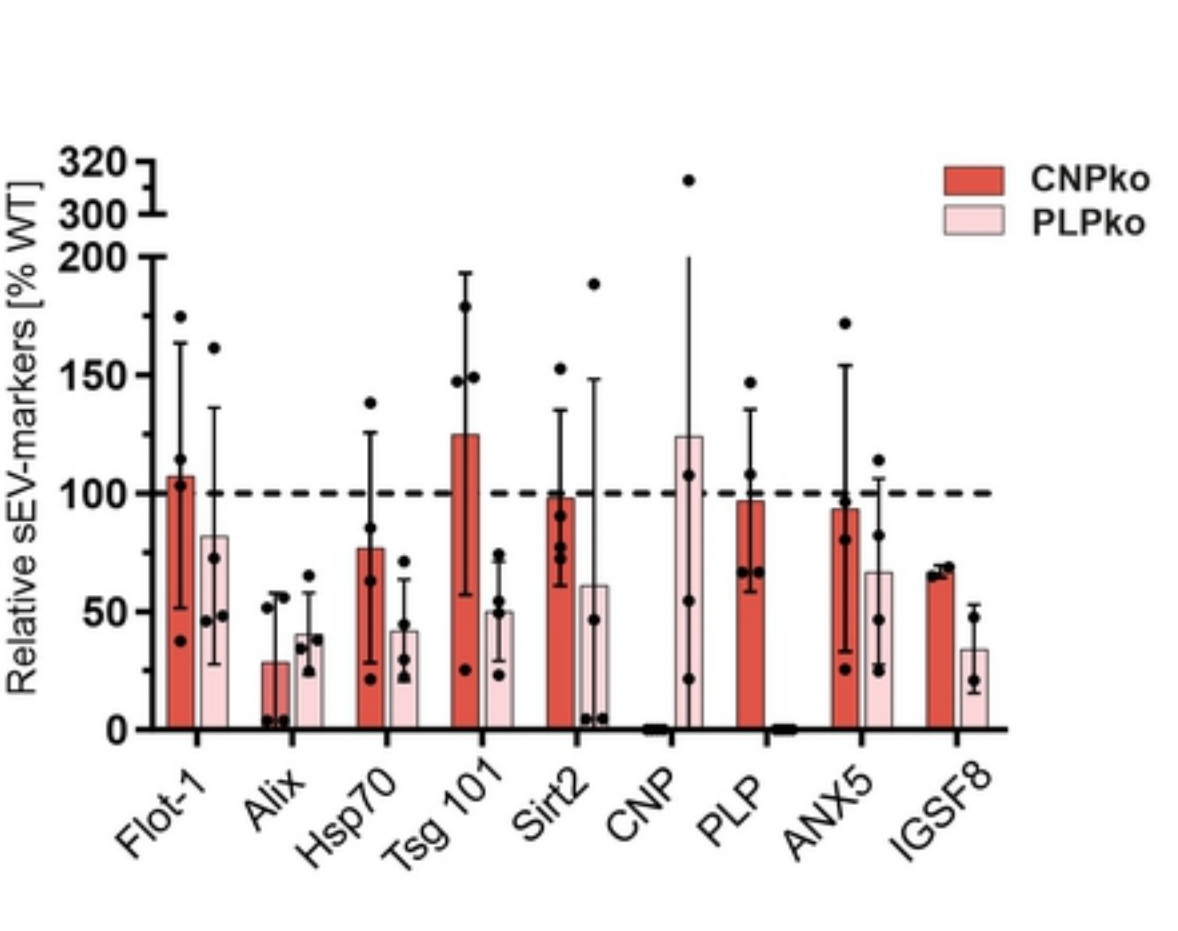

Figure 5

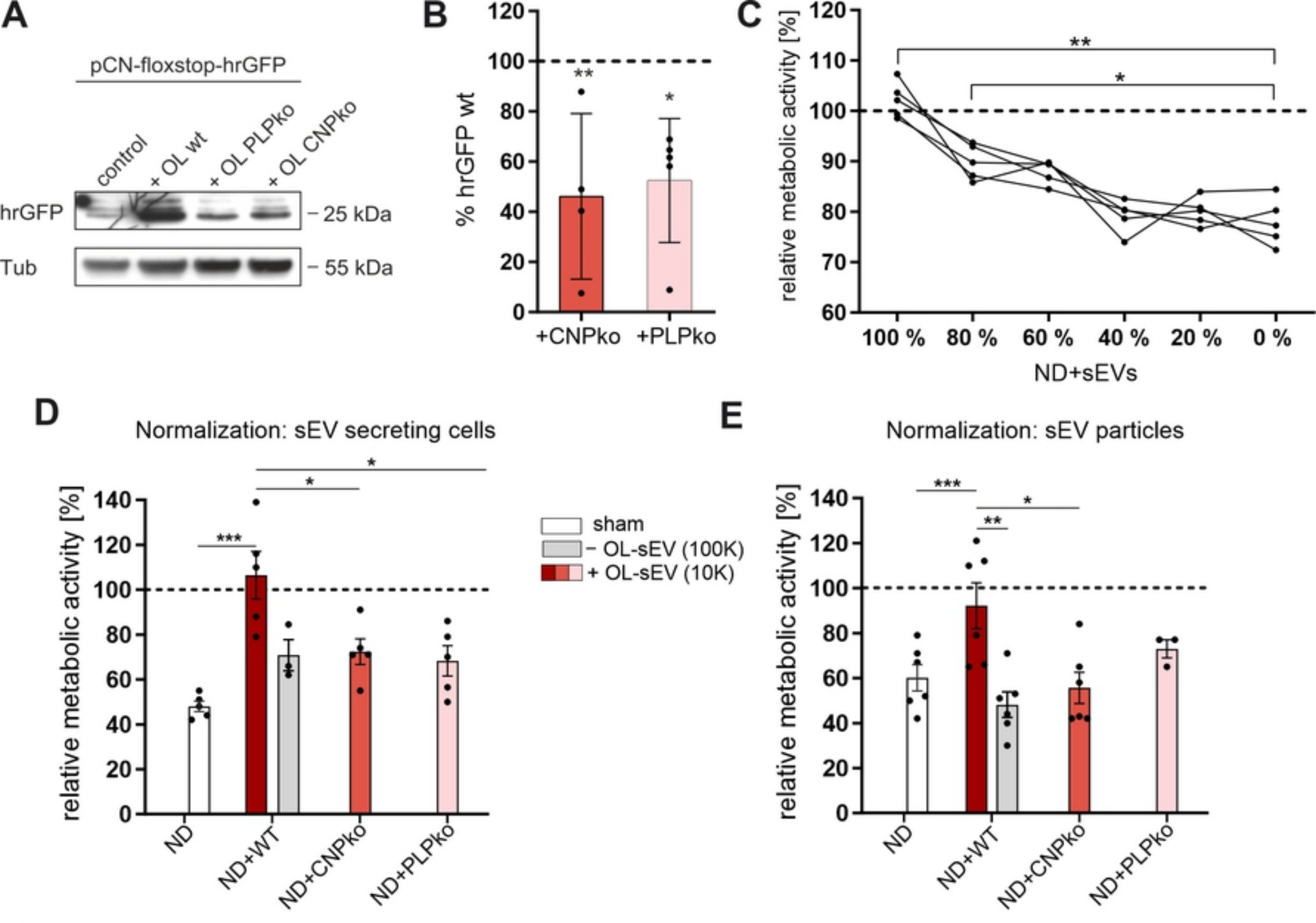
A
pCN-floxstop-hrGFP
control
+ OL wt
+ OL PLPko
+ OL CNPko
hrGFP
– 25 kDa
Tub
– 55 kDa
B
% hrGFP wt
+CNPko
+PLPko
C
relative metabolic activity [%]
100 %
80 %
60 %
40 %
20 %
0 %
ND+sEVs
D
Normalization: sEV secreting cells
relative metabolic activity [%]
sham
– OL-sEV (100K)
+ OL-sEV (10K)
ND
ND+WT
ND+CNPko
ND+PLPko
E
Normalization: sEV particles
relative metabolic activity [%]
ND
ND+WT
ND+CNPko
ND+PLPko

Figure 6

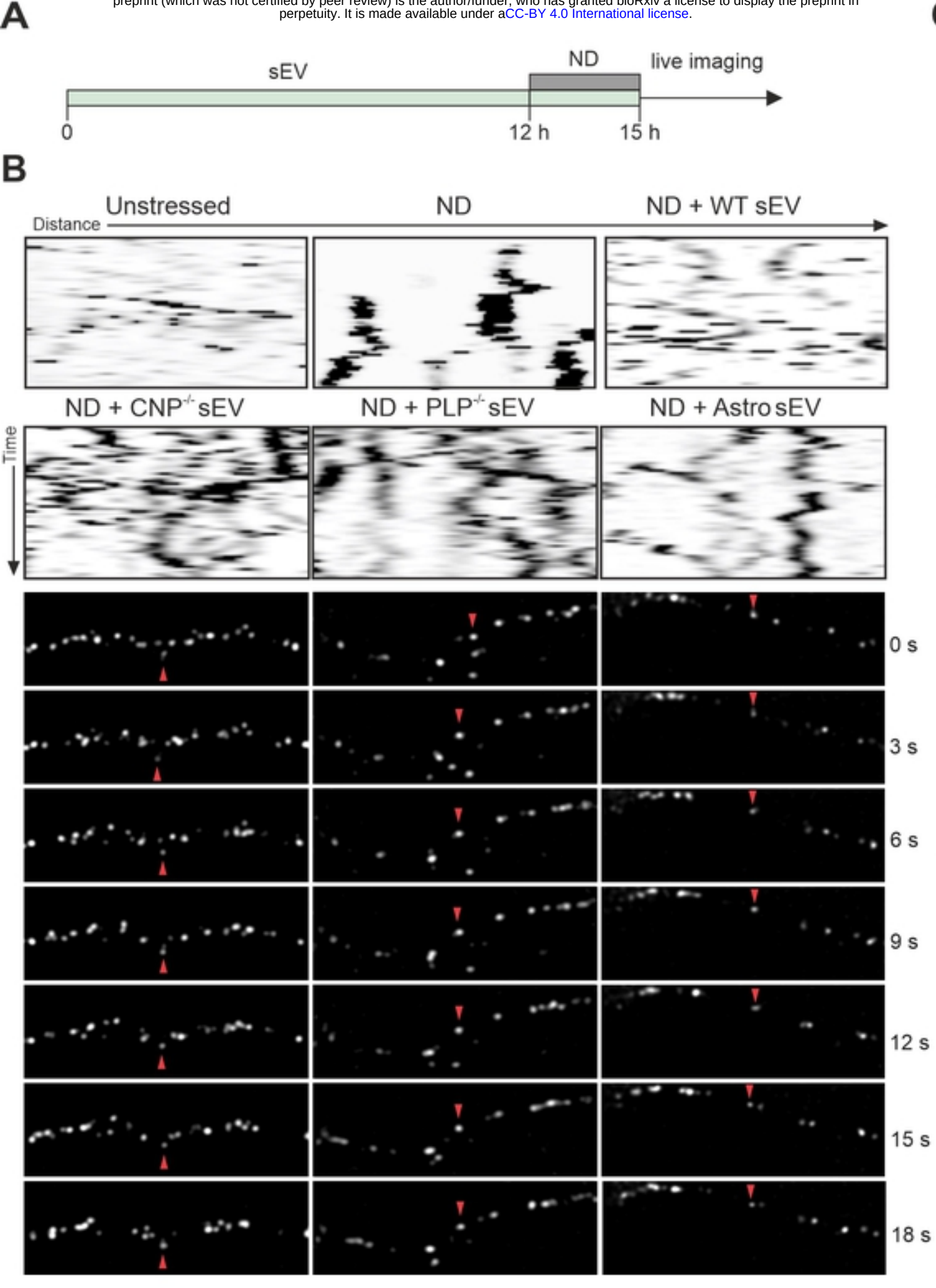

Figure 7